CAVITATION IN HORIZONTAL PIPELINES DUE TO WATER HAMMER*)

Report No. B/71/3

J.P.Th. Kalkwijk, senior scientific officer
C. Kranenburg, scientific officer
Delft University of Technology
Department of Civil Engineering
Laboratory of Fluid Mechanics

*) Sections INTRODUCTION through CONCLUSIONS of this report were also published in: The Journal of the Hydraulics Division, Proceedings ASCE, vol. 97, 1971, no. HY 10, Oct..

CONTENTS

INTRODUCTION

When designing a pipeline for the transport of a liquid one of the problems to be considered is the provision of a device to guard against low pressures. These low pressures can be caused, for example, by a sudden pump failure. The failure creates a negative pressure wave which travels in the downstream direction. Vapor pressure may be reached at a particular point, after which cavitation may occur in a long part of the pipeline. After a certain time the cavitation vanishes causing a very high pressure which may damage the pipeline. In order to prevent the development of cavities and consequently the development of high pressures, a device like an air vessel or surge tank is built. The presence of these devices decreases the pressure waves considerably and increases the time scale of the system. This general procedure for designing a pipeline is greatly influenced by the fact that the phenomenon of cavitation in a long pipeline is badly understood and experiments in this field are rare.

In the past, for a sudden pump failure or valve closure at the beginning of a pipeline the relevant pressures and velocities were determined by introducing into the computation a cavity behind the pump or valve. The formation of the cavity was governed by the continuity condition while in the pipeline itself the celerity of a pressure wave was not disturbed (Ref. 1).
The first authors who developed a more realistic model of the phenomenon, were de Haller and Bédué (Ref. 5). They pointed out that a negative pressure wave can give rise to cavities which occur along a great length of the pipeline. An important feature of the cavity was that its vertical cross-section remained small with respect to the total area of the cross-section. For an inclined pipeline the movement of the cavity and the liquid were greatly influenced by gravity. Siemons (Ref. 7), studying the cavitation in a horizontal pipe, used the idea of an extensive cavity to describe the formation and collapse of a long cavity in the top of the pipe. In his numerical solution to the problem, he applied the same grid for both the cavitation and the water hammer region and arrived in this way at fairly extensive cavities. However, a simple check of the results of his solution shows that the balance of mass at the boundary of the cavity is not fulfilled. Consequently the conclusion that no high pressures will occur after the collapse is not justified.

Dijkman and Vreugdenhil (Ref. 3) considered Siemons problem again and at the same time extended their study by considering the influence of gas escaping from the water at pressures below saturation pressure. They obtained very thin cavities (some millimeters) for a specific case, even if large amounts of gas are assumed to escape from the water. Considering the flow below the cavity as a free surface flow does not seem realistic from a practical point of view, since pipes generally do not lie perfectly horizontal. Nevertheless, their conclusion that escaping gas reduces the pressures after the collapse is valuable.
At this time (1971) the afore-mentioned mathematical studies have not been verified by experiments. Therefore, the studies of Brown (Ref. 2) are intersting, because his theory was verified by prototype experiments. He studied the problem of water column separation at a discrete point. Usual water hammer theory and experiment disagreed, and consequently small gas pockets were introduced at the grid points of the graphical computational scheme. In this way the overall celerity was decreased, especially at low pressures. By introducing certain assumptions on the total amount of gas in the pockets it was possible to obtain a close agreement between theory and experiment. In this case the gas had a detrimental effect on the water hammer transient.

The present paper extends the limited knowledge of the occurrence of cavitation in a horizontal pipeline by presenting a simplified computational procedure in which the idea of a single long cavity is abandoned. The computations are compared with experimental results.

PHENOMENON DESCRIPTION

Under normal circumstances, water hammer computations are based on the celerity of a disturbance in a pipe completely filled with water, namely

$$c_o = \left[\rho_o \left(\frac{1}{K} + \frac{n}{\delta/D E}\right)\right]^{-\frac{1}{2}} \qquad \ldots (1)$$

in which c_o = celerity of the disturbance, K = bulk modulus of the water, ρ_o = specific density of the water, δ = wall thickness of the pipe, E = bulk modulus of the pipe material, D = diameter of the pipe and n = coefficient accounting for anchorage system.
In these cases K is equal to $2 \cdot 10^9$ N/m^2, while for sewage pipelines a lower value for K is sometimes introduced. In this way the possible presence of small gas bubbles is taken into consideration. It is well known that gas bubbles, even in small quantities, considerably decrease the celerity c_o, which is generally kept constant in computations.
If the pressure in the water reaches vapor pressure, a certain moment cavitation is expected to occur. This means that vapor bubbles are formed as a consequence of the pressure reduction. In general this is called a cavitating flow. It is generally accepted that cavitation in liquids is induced by microsize nuclei. The nuclei cannot exist as free bubbles in the liquid because it can be shown that they must dissolve in the liquid, even when the liquid is supersaturated (Ref. 4). A requirement for the existence of nuclei is the solid phase. They will be present in crevices in dust particles or in the wall. At low pressures certain nuclei will grow to big vapor bubbles, which may rise to the highest point of the pipe. If the cavitation lasts for a long time, the vapor bubbles will finally form long cavities in the top of the pipe. Computations have to show whether this situation will be reached or not.

FIRST APPROACH TO THEORY

As explained before, nuclei, being small gas bubbles in the liquid, are necessary for cavitation to occur. It is obvious that they should be considered in a theoretical approach. However, due to the complex character of the nuclei it is not possible to take into account all their properties. Therefore, the first assumption is that there is no slip between nuclei and liquid. This implies that nuclei attached to the wall are not taken into consideration. The second assumption is that during the cavitation no gas will be released from the liquid into the vapor bubble. As the time

interval in which the vapor bubbles exist is short with respect to the time scale of the diffusion process (Ref. 6), this seems to be justified. The third approximation is that the gravitational influence is neglected. If the distribution of nuclei is uniform, then the distribution of vapor bubbles will be uniform as well. In reality this does not seem fully justified as the cavitation occurs mainly in the top of the pipe. Even when the vapor bubbles rise to the top of the pipe the consequences do not seem serious. The flow, which is in fact a two phase flow, is considered to remain homogeneous. Based on the assumptions mentioned before, the equations of continuity and motion for this flow can be derived.

Equation of continuity

Using the law of conservation of mass and ignoring the mass of the bubbles or nuclei, one obtains

$$\frac{\partial}{\partial x}(1 - k)\,\rho\, uA + \frac{\partial}{\partial t}(1 - k)\,\rho\, A = 0 \qquad \ldots (2)$$

in which (see Fig. 1) A = area of cross-section, u = fluid velocity, k = ratio of bubble volume to total volume, x = spacial coordinate, and t = time coordinate.
With the well-known relationship for A and ρ

$$dA = \frac{An}{\frac{\delta}{D}E}\,dp \qquad \ldots (3)$$

$$d\rho = \frac{\rho_o}{K}\,dp \qquad \ldots (4)$$

in which p = pressure, and ρ_o = specific density of fluid.
Eq. 2 transforms to

$$\frac{\partial}{\partial x}(1 - k)\,u + \frac{(1 - k)\,u}{\rho_o c_o^2}\frac{\partial p}{\partial x} - \frac{\partial k}{\partial t} + \frac{1 - k}{\rho_o c_o^2}\frac{\partial p}{\partial t} = 0 \qquad \ldots (5)$$

In Eq. 5, k is a function of pressure p. Assuming a constant number N of nuclei per unit of mass of fluid, all having the same radii R, one obtains

$$k = \frac{\frac{4}{3}\pi NR^3}{\frac{1}{\rho} + \frac{4}{3}\pi NR^3} \qquad \ldots (6)$$

If the gas bubble content is small then k can be approximated by

$$k = \frac{4}{3}\pi \rho NR^3 \qquad \ldots (7)$$

In Eq. 6 the bubble radius is determined by the equilibrium condition for a single bubble, in which dynamic effects are neglected. This is justified if only transient phenomena are considered which have a larger time scale than the natural period of oscillation of that bubble. If the bubble contains a certain amount of gas the equilibrium condition is

$$p - p_v + \frac{2\sigma}{R} - p_g = 0 \qquad \ldots (8)$$

in which p_v = vapour pressure in bubble, p_g = gas pressure in bubble, and σ = surface tension.
As the bubble is surrounded by a liquid at constant temperature, it is assumed that the gas in the small bubble behaves isothermally, in which case Boyle's gas law applies. Consequently

$$p_g R^3 = C = \text{contant} = p_o R_o^3 \qquad \ldots (9)$$

The suffix $_o$ represents a certain initial condition. Substitution into Eq. 7 yields

$$p - p_v + \frac{2\sigma}{R} - \frac{C}{R^3} = 0 \qquad \ldots (10)$$

A graphical representation of this relationship is given in Fig. 2. A radius of 10^{-5} m has been chosen for the initial nucleus under atmospheric pressure. According to Ref. 4, nuclei of this size are quite common, although much bigger bubbles are feasible in sewage water. If the bubble has attained a radius of

$$R = \sqrt{\frac{3\,C}{2\,\sigma}} \qquad \ldots (11)$$

no further pressure reduction occurs. The corresponding pressure is less than the vapor pressure p_v. It is believed that at this point cavitation really begins, because the continued growth of the bubble is unstable. However, if this situation is reached, explosive growth without bound is not possible due to the continuity condition for the fluid.
Eq. 5 still contains concentration k. By means of Eqs. 4 and 6 the derivatives of k with respect to x and t in Eq. 2 can be replaced by derivatives of p, using the product rule of differentiation

$$dk = \frac{dk}{dR} \cdot \frac{dR}{dp} \cdot dp = \frac{dk}{dR} \cdot \frac{1}{\frac{dp}{dR}} \cdot dp \qquad \ldots (12)$$

or

$$dk = \frac{3k}{\frac{2\sigma}{R} - \frac{3C}{R^3}}\, dp \qquad \ldots (13)$$

Substitution of this result into Eq. 5 yields, after some rearrangement

$$\frac{\partial p}{\partial t} + u \frac{\partial p}{\partial x} + f \frac{\partial u}{\partial x} = 0 \qquad \ldots (14)$$

with

$$f = \left[\frac{1}{\rho_o c_o^2} + \frac{3k}{(1-k)\left(\frac{3C}{R^3} - \frac{2\sigma}{R}\right)} - \frac{k}{K}\right]^{-1} \qquad \ldots (15)$$

For small k this can be simplified to

$$f = \left[\frac{1}{\rho_o c_o^2} + \frac{3k}{\frac{3C}{R^3} - \frac{2\sigma}{R}}\right]^{-1} \qquad \ldots (16)$$

Equation of motion

Application of the law of conservation of momentum to element dx of the pipeline yields

$$\frac{\partial}{\partial t} \rho (1-k)\ uA + \frac{\partial}{\partial x} \rho\ (1-k)\ u^2 A + A \frac{\partial p}{\partial x} = -\ AW \qquad \ldots\ (17)$$

in which W represents friction. As only small quantities of gas are considered, a usual quadratic friction law is assumed, i.e.

$$W = \frac{\lambda}{2D} \rho_o u \mid u \mid \qquad \ldots\ (18)$$

in which λ = friction parameter. After some evaluation, using the equation of continuity, Eq. 17 transforms to

$$\frac{\partial u}{\partial t} + u \frac{\partial u}{\partial x} + \frac{1}{\rho_o (1-k)} \frac{\partial p}{\partial x} = -\ \frac{W}{\rho_o (1-k)} \qquad \ldots\ (19)$$

Transformation to characteristic coordinates

The equations of continuity and motion are of the quasilinear hyperbolic type. This means that the equations can be solved by the method of integration along characteristics. The characteristics are given by

$$\frac{dx}{dt} = u \pm \sqrt{\frac{f}{\rho_o (1-k)}} = u \pm c \qquad \ldots\ (20)$$

while along these characteristics

$$du \pm \frac{dp}{\sqrt{\rho_o (1-k) f}} = -\ \frac{W}{\rho_o (1-k)}\ dt \qquad \ldots\ (21)$$

In Eq. 12, c represents the celerity of an infinitesimal disturbance, depending on f and k and consequently on the fluid pressure p. The relationship between p and c is shown in Fig. 3, where some curves are drawn for some different initial conditions, namely c_o = 500 and 1000 m/s, bubble sizes R_o of 10^{-4} and 10^{-6} m at p = 10^5 N/m^2 (atmospheric

pressure) and concentrations k_o of 4.10^{-4} and 4.10^{-6} at $p = 10^5$ N/m^2. The vapor pressure was kept constant at a value of $p_v = 2.10^3$ N/m^2.

The formula for c and the relevant curves show the following features:

a. Under atmospheric pressure c has already decreased considerably with respect to c_o for the high concentration $k_o = 4.10^{-4}$, while a concentration $k_o = 4.10^{-6}$ does not have this effect; moreover, the initial bubble size R_o has a noticeable influence.

b. When the pressure decreases the influence of c_o becomes smaller and the curves with the same concentration k_o approach each other.

c. Finally, at a certain low pressure the influence of the concentration k_o vanishes and the celerity c tends to zero. This value is reached if f = 0, while the corresponding bubble radius is given by Eq. 11. Continued growth of the bubble yields negative values for f and consequently imaginary characteristics. This indicates that the system of equations has become elliptic with independent variables x and t. This is impossible from a physical point of view, so that then the phenomenon has to be described in a different way.

Physical system with unstable bubbles

Consider, as before, a fluid with a homogeneous distribution of stable bubbles of equal size and investigate the behavior of a portion of this fluid between two close cross-sections attached to the fluid particles. After pressure reduction in this region the bubbles between the two cross-sections are going to grow. At a certain moment the bubbles reach the critical size where they tend to become unstable. Continued bubble growth will lead to a situation where all bubbles are unstable. Introducing a small disturbance, it can be shown that only one bubble continues its growth, while the other bubbles return to their stable position. This can happen without change in the total volume of the region considered, but during the process the pressure tends to vapor pressure p_v. The greater the number of bubbles the closer the pressure tends to p_v. Further growth of the unstable bubble does not cause considerable pressure fluctuations.

So far a local phenomenon has been considered. However, this occurs in a big part of the pipeline and a situation arises with many unstable bubbles,

which act like "negative" springs. The pressure is close to p_v. Again assuming a constant total volume it can be proved that in the long run only one unstable bubble can remain; however, in practical circumstances this final state will not be reached. Which bubble will grow is unpredictable. During this process, inertia and friction effects play an important role. The computations from which these conclusions result are not shown herein. The conclusions are

a. In the cavitation stadium a limited number of bubbles will grow. The assumption of a homogeneous bubble distribution is no longer justified.
b. The equations derived before can no longer be used. Due to the erratic character of the phenomenon, a stochastic approach is in fact required.
c. The pressures at all points where cavitation occurs tend to vapor pressure.

Despite the fact that these conclusions are drawn for the academic case of bubbles of equal size they hold as well for fluids with bubbles of different sizes. In that case the biggest bubbles are going to grow.

SECOND APPROACH TO THEORY

Region without cavitation

In a preceding section it was shown that, under most circumstances the celerity is equal to c_o, provided the bubble content is not too high. Thus, for the case $p > p_v$ the bubbles are assumed to play no role. The simplified relevant equations are

$$\frac{\partial p}{\partial t} + \rho_o c_o^2 \frac{\partial u}{\partial x} = 0 \qquad \ldots (22)$$

and

$$\frac{\partial u}{\partial t} + \frac{1}{\rho_o} \frac{\partial p}{\partial x} = - \frac{\lambda}{2D} u|u| \qquad \ldots (23)$$

Making use of the characteristic coordinates with

$$\frac{dx}{dt} = \pm c_o \qquad \ldots (24)$$

these equations transform to

$$\frac{du}{dt} \pm \frac{1}{\rho_o c_o} \frac{dp}{dt} = - \frac{\lambda}{2D} u|u| \qquad \ldots (25)$$

Eqs. 24 and 25 can be easily solved by means of numerical calculus.

Region with cavitation

As pointed out before, it is assumed that $p = p_v$. Consequently Eqs. 5 and 19 become

$$\frac{\partial k}{\partial t} + u \frac{\partial k}{\partial x} = (1 - k) \frac{\partial u}{\partial x} \qquad \ldots (26)$$

$$\frac{\partial u}{\partial t} + u \frac{\partial u}{\partial x} = - \frac{\lambda}{2D} u|u| \qquad \ldots (27)$$

As $k << 1$, Eq. 26 simplifies to

$$\frac{\partial k}{\partial t} + u \frac{\partial k}{\partial x} = \frac{\partial u}{\partial x} \qquad \ldots (28)$$

The characteristics of the quasilinear equations of first order 27 and 28 are given by

$$dt = \frac{dx}{u} = - \frac{2D}{\lambda} \frac{du}{u|u|} \qquad \ldots (29)$$

and

$$dt = \frac{dx}{u} = \frac{dk}{\frac{\partial u}{\partial x}} \qquad \ldots (30)$$

respectively. The first equality in Eqs. 29 and 30 indicates that a disturbance propagates with the fluid velocity; the velocity of propagation with respect to the fluid particles has reduced to zero. Integration of Eq. 29, which affords the integral surface of Eq. 27, yields

$$x - x_i = - \frac{2D}{\lambda} \frac{u_i}{|u_i|} \log \left| \frac{u}{u_i} \right| \qquad \ldots (31)$$

and

$$t - t_i = \frac{2\,D}{\lambda}\left(\frac{1}{|u|} - \frac{1}{|u_i|}\right) \qquad \ldots (32)$$

in which $x_i = x_i(t_i)$ and $u_i = u_i(t_i)$ represent the initial conditions of the cavitation region. In Eq. 30 $\frac{\partial u}{\partial x}$ can be derived from Eqs. 31 and 32. These equations in differential form are

$$dx - \frac{dx_i}{dt_i}\,dt_i = \frac{2\,D}{\lambda}\left(-\frac{du}{|u|} + \frac{1}{|u_i|}\,\frac{du_i}{dt_i}\,dt_i\right) \qquad \ldots (33)$$

$$dt - dt_i = \frac{2\,D}{\lambda}\left(-\frac{du}{u|u|} + \frac{1}{u_i|u_i|}\,\frac{du_i}{dt_i}\,dt_i\right) \qquad \ldots (34)$$

The meaning of dx_i and dt_i is shown in Fig. 4. They represent the differential form of the curve at which the initial condition u_i is given. Taking $dt = 0$ one obtains:

$$du = \frac{\partial u}{\partial x}\,dx \qquad \ldots (35)$$

Together with the preceding equations, and after elimination of dx

$$\frac{\partial u}{\partial x} = \frac{\dfrac{1}{u_i|u_i|}\,\dfrac{du_i}{dt_i} + \dfrac{\lambda}{2\,D}}{\dfrac{1}{|u|}\left(\dfrac{1}{u}\,\dfrac{dx_i}{dt_i} - 1\right) + \dfrac{2\,D}{\lambda}\,\dfrac{1}{|uu_i|}\,\dfrac{du_i}{dt_i}\left(\dfrac{1}{u} - \dfrac{1}{u_i}\right)} \qquad \ldots (36)$$

In this way $\frac{\partial u}{\partial x}$ has been expressed in the initial conditions at $x_i = x_i(t_i)$ and variable velocity u.

If, in Eqs. 30 and 36, u is replaced by the result of Eq. 32 then Eq. 30 can be integrated, yielding the integral surface of Eq. 28

$$k = \log\left[1 + \frac{\dfrac{du_i}{dx_i} + \dfrac{\lambda}{2\,D}\,\dfrac{u_i|u_i|}{\dfrac{dx_i}{dt_i}}}{1 - \dfrac{u_i}{\dfrac{dx_i}{dt_i}}} \cdot \frac{t - t_i}{1 + \dfrac{\lambda}{2\,D}\,|u_i|\,(t - t_i)}\right] \qquad \ldots (37)$$

and

$$x - x_i = \frac{2\,D}{\lambda} \frac{u_i}{|u_i|} \log \left[1 + \frac{\lambda}{2\,D} |u_i| \, (t - t_i) \right] \qquad \ldots (38)$$

Eq. 38 could also have been derived from Eqs. 31 and 32 by eliminating u. It describes the path of a disturbance and, because of the vanished celerity, the path of a fluid particle. In a parameter form Eqs. 37 and 38 give the relative vapor volume k as a function of x and t in the cavitation region.

Transition from region without cavitation to region with cavitation

In the foregoing analysis two regions have been distinguished, one without cavitation in which the celerity is equal to c_o, and another with cavitation, where the velocity of propagation becomes zero. Consequently in the cross-section of transition a sudden change of the celerity occurs. The laws of conservation of mass and momentum must hold for the region of transition as well. They yield the relation between pressures and fluid velocities on both sides of the transition, as well as an expression for the celerity of the discontinuity.
Fig. 5 gives a definition sketch of the situation in the transitional region. Subscript $_f$ stands for the fluid without cavitation, while subscript $_v$ stands for the fluid with cavitation. The transition between the two regions moves with a velocity c_s' with respect to the pipe wall. If the laws of conservation of mass and momentum are applied to the region, enclosed by cross-sections a and b and the pipe wall, the results are

$$(c_s' - u_f)\, \rho_f A_f - (c_s' - u_v)\, (1 - k)\, \rho_v A_v = 0 \qquad \ldots (39)$$

and

$$(c_s' - u_f)\, \rho_f A_f u_f - (c_s' - u_v)\, (1 - k)\, \rho_v A_v u_v = A_v\, (p_f - p_v) \qquad \ldots (40)$$

Substituting

$$\rho_f A_f = \left(1 + \frac{p_f - p_v}{\rho_o c_o^2}\right) \rho_v A_v, \quad \Delta p = p_f - p_v, \quad \text{and } \rho_v \approx \rho_o$$

into Eqs. 39 and 40 one obtains

$$\left(1 + \frac{\Delta p}{\rho_o c_o^2}\right) (c_s' - u_f) - (1 - k)(c_s' - u_v) = 0 \qquad \ldots (41)$$

$$\left(1 + \frac{\Delta p}{\rho_o c_o^2}\right) (c_s' - u_f) u_f - (1 - k)(c_s' - u_v) u_v = \frac{\Delta p}{\rho_o} \qquad \ldots (42)$$

Introducing celerity c_s of the transition with respect to the fluid particles in the region without cavitation, one obtains from Eq. 41:

$$c_s = c_s' - u_f = \frac{(1 - k)\,\Delta u}{k + \frac{\Delta p}{\rho_o c_o^2}} \qquad \ldots (43)$$

in which $\Delta u = u_f - u_v$. If $k \ll 1$, Eq. 43 may be approximated by

$$c_s = \frac{\Delta u}{k + \frac{\Delta p}{\rho_o c_o^2}} \qquad \ldots (44)$$

Multiplication of Eq. 41 with u_v and subtraction from Eq. 42 yields

$$\Delta p = \rho_o \left(1 + \frac{\Delta p}{\rho_o c_o^2}\right) c_s \Delta u \qquad \ldots (45)$$

As $\frac{u_o}{c_o} \ll 1$ and consequently $\frac{\Delta p}{\rho_o c_o^2} \ll 1$, Eq. 45 may be approximated by

$$\Delta p = \rho_o c_s \Delta u \qquad \ldots (46)$$

Replacing c_s in Eq. 46 by the right-hand size of Eq. 31 gives

$$(\Delta u)^2 = \frac{\Delta p}{\rho_o} \left(k + \frac{\Delta p}{\rho_o c_o^2}\right) \qquad \ldots (47)$$

Finally, elimination of Δu from Eqs. 44 and 47 yields

$$c_s = c_o \left[1 + k \frac{\rho_o c_o^2}{\Delta p} \right]^{-\frac{1}{2}} \qquad \ldots (48)$$

A particular requirement of the foregoing analysis is that $\Delta p > o$ and hence c_s and Δu have the same sign. However, rarefaction shocks ($\Delta p > o$, $\Delta u < o$ and $c_s < o$) are not acceptable as this would imply a gain of the mechanical energy across the shock. Therefore, the condition for the existence of a shock reads

$$\Delta u > o \qquad \ldots (49)$$

When cavitation starts in some cross-section, $k = o$, $\Delta u = o$ and $\Delta p = o$ in that cross-section. In that case c_s cannot be determined from Eqs. 43 through 48, but it depends on the water hammer equations and the condition $p = p_v$. The combination $k > o$, $\Delta u = o$, $\Delta p = o$ can be shown to be impossible.

Conclusions to foregoing sections

In an arbitrary case, one can distinguish between regions with and without cavitation. Eqs. 24 and 25 describe the behavior of the flow in the region without cavitation. Eqs. 31 and 32 describe the behavior of the velocity in the region with cavitation, while Eqs. 37 and 38 give the corresponding concentration of vapor. Between the two regions a continuous transition or a shock exists. The changes of the velocity and pressure at the transition are related by Eq. 47 and the celerity of the shock is given by Eq. 48. In a computation, characteristics of the type $\frac{dx}{dt} = u$ (cavitation) and $\frac{dx}{dt} = \pm c_o$ (no cavitation) will intersect (Fig. 6). At the intersection the velocity u_v and the concentration k in the region with cavitation can be derived from Eqs. 31, 32 and 37. Eq. 25 and Eq. 47 yield the two unknowns p_f and u_f.
Afther this analysis of the problem a PL1-program, which is described in Appendix 1, was set up in order to solve the equations numerically. At the same time a model was constructed to check the applicability of the theory.

EXPERIMENT

Description of model

Fig. 7 gives a schematic sketch of the model. It consists of a p.v.c. pipeline (D = 0.0814 m, δ = 0.0043 m, E $\approx$ 2.2 * 10^9 N/m^2) having a total length of 200 m. The pipeline is horizontal. A vertical pipe with a length of 2 m has been connected to the pipeline at the end. Due to spacial limitations the pipeline has been folded up. Under stationary circumstances the water is discharged in a low head reservoir. In the latter reservoir a small flume with V-notch has been fitted for flow measurement in the stationary situation. During an experiment, the level in the low head reservoir can be considered as being constant. The maximum fall between the water levels in the two reservoirs is approximately equal to 2 m.
A pump supplies water from the low head reservoir to the high head reservoir. The flow can be controlled by two valves located at the pressure side of the pump and at the end of the test pipeline. The maximum water velocity which can be attained amounts to 1 m/s. In the stationary situation the pressure in the pipeline decreases linearly. Some measurements gave a friction coefficient λ = .0194 and a water hammer celerity c_o = 430 m/s. In the high head reservoir a piston valve has been positioned. In order to avoid disturbances the piston valve can move freely over a short distance in the pipe. In this way the valve attains the water velocity.
Finally the valve meets a ceiling which stops the valve practically instantaneously. During an experiment at several points of the pipeline the behavior of the pressure can be measured with flush mounted pressure transducers. The other electronic equipment consists of four measurement amplifiers, a galvanometer drive, and a u.v. recorder. The pressure transducers have the lowest natural frequency of all electronic equipment, namely 1000 c/s.

Description of experiment

After the closure of the piston valve the pressure behind the valve decreases immediately to vapor pressure. The corresponding fluid velocity does not reduce to zero and consequently a large cavity begins to develop behind the

valve. The negative pressure wave propagates in downstream direction with a celerity to 430 m/s, and as soon as this wave has passed, bubbles are going to grow. At the beginning of the pipeline the front of the pressure wave is very steep, but depending on distance, the slope decreases. This indicates that dispersion could be observed for pressures below atmospheric pressure.

Fig. 8, representing some pressure graphs at varying locations of the pipe, shows this phenomenon. When the negative pressure wave meets the end of the pipeline with the constant head reservoir the wave is reflected negatively. At this moment cavitation can be observed in the whole pipeline. The reflected positive pressure wave enters the region with cavitation bubbles with a celerity which is much lower than the normal water hammer celerity. In the reflected wave front a vertical part (shock) develops. After the collapse of the vapor bubbles, small gas bubbles remain behind at several places. This implies that the gas content of the fluid plays a certain role. After the wave front has passed the cavitation region it meets the big cavity behind the valve, while all cavitation in the rest of the pipeline has vanished.

In the big cavity, the pressure remains low and the wave front is negatively reflected again. As the initial fluid velocity is high enough it keeps the same direction and the big cavity continues its growth. After the reflection of the wave against the big cavity, cavitation no longer occurs in the pipeline. The height of the wave decreases considerably, and depending on the initial conditions the wave damps out completely. Finally the water in the pipeline behaves as a rigid water column.

During this process the fluid velocity changes its direction, the big cavity becomes smaller and closes again. At the moment of closure of the big cavity a high pressure arises. As the follow-up of the process is not interesting, the experiment was stopped here. As an example it can be mentioned that in the case of an initial velocity u_o = .95 m/s the big cavity exists during 4.0 sec., while its maximum length was less than 10 m. The bubble cavitation region in the pipe is shown in Fig. 9; the maximum duration of cavitation amounts to 1.2 sec. and occurs at the beginning of the pipeline.

Computation

The origin of the x-axis is chosen at the beginning of the pipeline; the origin of the t-axis at the moment of valve closure. Assume that after valve closure a sudden pressure drop arises. The initial curve where cavitation begins is then defined by

$$\frac{dx_i}{dt_i} = c_o \qquad \ldots (50)$$

After the passage of the pressure wave the velocity along this curve becomes

$$u_i = u_o - \frac{1}{\rho_o c_o}(p_L - p_v) - \frac{\lambda}{2D}\frac{u_o^2}{c_o}(L - c_o t_i) \qquad \ldots (51)$$

in which u_o = velocity in stationary circumstances, and p_L = pressure of low head reservoir. This yields for the derivative of u_i with respect to t_i

$$\frac{du_i}{dt_i} = \frac{\lambda}{2D} u_o^2 \qquad \ldots (52)$$

The concentration k becomes

$$k = \log\left[1 + \frac{\lambda}{2D} \cdot \frac{u_i^2 + u_o^2}{c_o - |u_i|} \cdot \frac{t - t_i}{1 + \frac{\lambda}{2D}|u_i|(t - t_i)}\right] \qquad \ldots (53)$$

By means of Eq. 30 and the condition $u_i << c_o$ this expression changes to

$$k \approx \left(1 - \frac{u}{u_i}\right)\frac{u_i^2 + u_o^2}{c_o |u_i|} \qquad \ldots (54)$$

in which

$$u = \frac{u_i}{1 + \frac{\lambda}{2D}|u_i|(t - t_i)} \qquad \ldots (55)$$

Although the numerical program allows a less restricted shape of the pressure drop, a computation has been made by means of the last two relationships. The results of such a computation for the case $u_o = 0.97$ m/s and $p_L = 8.2 \times 10^4$ N/m^2 are shown in Fig. 9 (x,t-diagram), Fig. 10 (p.u-diagram), and in Fig. 8 (pressure behavior for some locations). These numerical results can be checked by a further analytical approximation. Neglecting friction, integration along a characteristic in the region without cavitation yields the following relationship between pressures and velocities at the shock and at x = L

$$\frac{p_v + \Delta p}{\rho_o c_o} - u_f \approx \frac{p_L}{\rho_o c_o} - u_L \qquad \ldots (56)$$

As the pipeline is relatively short u_L can be approximated by

$$u_L \approx u_o - 2 \frac{p_L - p_v}{\rho_o c_o} \qquad \ldots (57)$$

Substitution of this result into the foregoing equation yields

$$\frac{\Delta p}{\rho_o c_o} \approx 3 \frac{p_L - p_v}{\rho_o c_o} - u_o + u_f \qquad \ldots (58)$$

Using this relationship the shock relations can be solved. The results are

$$c_s \approx \frac{c_o}{1 + k \frac{c_o}{u'}} \qquad \ldots (59)$$

and

$$\Delta p \approx \rho_o c_o \frac{u'}{2 + k \frac{c_o}{u'}} \qquad \ldots (60)$$

in which

$$u' = u_v - u_o + 3 \frac{p_L - p_v}{\rho_o c_o} \qquad \ldots (61)$$

Together with the equation for k and an estimation for $t - t_i$ the height and celerity of the shock can be computed. If some contributions of minor importance are neglected one obtains

$$c_s \approx \frac{c_o}{1 + \frac{\lambda}{D} \cdot \frac{\rho_o u_o^2}{p_L - p_v} (L - x)} \qquad \ldots (62)$$

and

$$\Delta p \approx \frac{p_L - p_v - \frac{\lambda}{4D} \rho_o u_o^2 (L - x)}{1 + \frac{\lambda}{2D} \cdot \frac{\rho_o u_o^2}{p_L - p_v} (L - x)} \qquad \ldots (63)$$

The analytical results for c_s and Δp agree very well with the numerical results.

Comparison of the results of computation and experiment

After valve closure, several phases of the process may be distinguished, i.e.:

a. At the beginning of the pipeline a negative pressure wave with a vertical front has been generated. During the propagation through the pipeline this front does not remain vertical, but it transforms gradually, probably due to the growth of nuclei. In the case shown in Fig. 8 at the end of the pipeline the front has a length of about 40 m. The computation does not show this dispersion effect; the front of the pressure wave remains vertical. This implies that the initial curve of the cavitation region in the experiment does not follow the theoretical curve. Both curves are shown in Fig. 9.

b. At the end of the pipe the negative pressure wave is reflected negatively. This implies that in the model cavitation ends at $x \approx 160$ m, while theoretically the end of the region is at $x = 200$ m. Fig. 8, e.g., shows that cavitation does not occur at all at $x = 180$ m.
From the location $x \approx 160$ m in the experiment a shock builds up gradually and is followed by a positive wave. The total height of the shock and

pressure wave agree reasonably with the computed shock. It is surprising that the path of the calculated shock and the shock in the model agree very well (Fig. 9). At the beginning of the pipe, say at x = 34 m (Fig. 8), the shock is fully developed and the height and the celerity agree well with the computed quantities. Finally the shock enters the region of the big cavity at the beginning of the pipe. This cavity shows a greater influence on the shock path than has been assumed. One of the reasons might be that the front of the cavity is not vertical. The free surface of the cavity is extended over several metres.

c. At the big cavity a negative reflection of the shock occurs. In the model the reflected negative pressure wave has a gentle slope which is in contrast to the results of the computation. Calculations and experiment both show that an extensive cavitation region does not occur again. The pressure wave goes on propagating through the pipeline. Fig. 8 shows that the time of occurrence agrees well with the computational results. However, the pressure waves in the model are heavily damped out. As the computations indicate, this cannot be caused by wall friction. Probably the dispersion which already played a role at the beginning of the process causes this effect. Moreover, the influence of gas evacuated from the liquid in the course of time is unknown.

d. The calculated and experimental closure times of the big cavity at the beginning of the pipeline agree very well. This is not shown in Fig. 8.

CONCLUSIONS

In the foregoing sections two attempts have been made to describe the phenomena that play a role if pressures are reduced to vapor pressure as a consequence of water hammer.

The first approach, based on the behavior of nuclei or gas bubbles, failed at the point where the radii of the bubbles exceed a critical value. At this size the bubbles become unstable and apparently the characteristics become imaginary. From this critical point the equations can no longer describe the process. The advantage of this theoretical approach was that it showed a considerable decrease of the velocity of propagation at low pressures. As this happened in the experiments too, this theory certainly holds to some extent.

The second approach, being in fact a crude schematization of the problem, distinguished between regions with and without cavitation. In the first region the celerity was reduced to zero, while in the other section the undisturbed celerity was supposed to hold. As the experiment shows, this method gives a reasonable description of the overall behavior of the process. Problems arose when it appeared that dispersion of the pressure waves changed the position and the time of occurrence of the cavitation region and the height of the shock. After the extensive cavitation had disappeared the remaining pressure waves were much more pronounced in the computation than they were in the experiment.

The next step for investigation might be a combination of both theories. Moreover, the role of the gas evacuating from the liquid has to be investigated in more detail.

RESULTS OF NUMERICAL COMPUTATIONS

A number of computations has been carried out for a simple pipeline system, which is shown in Fig. 14a. A pump transports a liquid through a horizontal pipeline from a low head reservoir to a high head reservoir. The levels of the reservoirs are assumed to be constant.
In order to reduce the number of parameters of the system, a sudden shut-down of the pump was replaced by a prescribed pressure drop, depending linearly on time:

$$p(0,t) = \begin{cases} p_o & , \quad t < 0 \\ p_o - (p_o - p_1)\,\frac{t}{\tau}, & 0 \leq t \leq \tau \\ p_1 & , \quad t > \tau \end{cases}$$

in which p_1 represents the pressure of the low head reservoir. The pressure difference $p_o - p_1$ and the time interval τ were chosen in such a manner that cavitation in the pipeline would occur.
The initial conditions for the computations were the steady state conditions.
Introducing dimensionless quantities

$$\bar{x} = \frac{x}{L}, \quad \bar{t} = \frac{c_o t}{L}, \quad \bar{p} = \frac{p}{p_o}, \quad \bar{u} = \frac{u}{u_o}$$

one obtains four dimensionless parameters describing the system:

$$\alpha = \frac{p_o - p_h}{p_o}, \quad \beta = \frac{p_o}{\rho_o c_o u_o}, \quad \gamma = \frac{c\tau}{L}, \quad \phi = \frac{p_o - p_1}{p_o}$$

in which p_h represents the pressure of the high head reservoir.
Parameters γ and ϕ result from the boundary condition at $x = 0$, representing the shut-down of the pump.
In fact a fifth parameter, viz. $\frac{u_o}{c_o}$, exists, but it disappears from the equations if the convective terms in the equations of motion and continuity which contain this small parameter, are neglected.
The computations were carried out for subjoined values of the parameters (42 cases).

ϕ	0.9	0.8	0.7	
α	0.8	0.6		all combinations
β	1.0	0.5	0.25	
γ	0.4	0.2		

ϕ	0.9			
α	0.4			all combinations
β	1.0	0.5	0.25	
γ	0.4	0.2		

The distance step was 0.02 L. All computations were ended at $0.2\ ^{L}/c_o$ after closure of the cavitation region.
A typical example of the results of the computations is given in Figs. 11a through 11e, which show a x,t-diagram of the cavitation region and a number of successive p,x-diagrams for the case

$$\alpha = 0.8, \quad \beta = 0.25, \quad \gamma = 0.2, \quad \phi = 0.9$$

Three other examples are given in Figs. 12a, b and c, in which only the x,t-diagram and the p,x-diagram at $0.2\ ^{L}/c_o$ after the closure of the cavitation region are inserted.
At the moment of closure of the cavitation region a pressure rise is generated which starts to propagate in both directions in the pipeline. The two resulting pressure waves, generally having different magnitudes, propagate up to the beginning and the end of the pipeline with only a slight deformation. At the beginning or the end of the pipeline the maximum pressure after cavitation occurs.
The magnitudes of the pressure waves $^{\Delta p}/p_o$ at $0.2\ ^{L}/c$ after closure are plotted in Fig. 13 for all cases computed.
On the left side of the discontinuity some curves show, the maximum pressure occurs at the beginning of the pipeline, in all other cases it occurs at the end. Neglecting the wave deformation, in the former case the maximum pressure, p_{max}, after cavitation is given by

$$\frac{p_{max}}{p_o} \approx 1 - \phi + \frac{\Delta p}{p_o}$$

and in the latter case

$$\frac{p_{max}}{p_o} \approx 1 - \alpha + \frac{\Delta p}{p_o}$$

Making use of these relations, the maximum pressure after cavitation are found to be less than the maximum steady state pressure in all cases considered. As the numerical program is believed to represent the physical phenomena to some extent, this result indicates that the consequences of cavitation in pipelines of the present type are not serious, as far as the maximum water hammer pressures are considered.

ACKNOWLEDGEMENTS

This paper is a report on a research program carried out at the Laboratory of Fluid Mechanics of the Department of Civil Engineering of the Delft University of Technology. The writers are grateful to J.C. van Winkelen who conducted the experiments.

APPENDIX 1 - The numerical program

by C. Kranenburg and E.O.F. Calle

General description

The program has been developed for the afore-mentioned pipeline system, depicted in Fig. 14a.
In order to avoid unnessary complications, a shut-down of the pump, which may cause cavitation in some part of the pipeline, has been replaced by a prescribed time-dependent pressure drop at the beginning of the pipeline.
The program is restricted to those cases in which only one cavitation region occurs at the same time. Very often, the pressure course due to a shut-down of a pump will fulfil this condition.
The initial conditions of the computation are given by the steady state conditions. Other boundary and initial conditions can be introduced in a simple way, e.g. for the experimental model, but extension of the program to more than one cavitation region at the same time will be more laborious.
The computation starts from the initial conditions and proceeds row by row in a fixed computational lattice by integration along characteristics. On both sides of each second row boundary conditions are necessary. So long as no cavitation occurs a row extends over the total length of the pipeline, but when a cavitation region does exist the part of the row inside the cavitation region is excluded from the water hammer computation. The boundary conditions for the remaining two parts of the row are those on both sides of the pipeline and the shock conditions on each side of the cavitation region. On the other hand the water hammer equations afford a relation which is necessary for the computation of the shock waves ("shock fitting"). Inside the cavitation region the afore-mentioned analytical solution is used, giving the remaining relations for the computation of these shock waves. When the shocks meet they change to two pressure waves in the water hammer region. See Fig. 14c. A simplified flow chart of the program is given in Fig. 15.
In conclusion of this section some specific details of the program will be described.

Water hammer computations

The method of characteristics has been chosen for the integration of the water hammer equations, because in this case the flow velocity is much less than the celerity, and hence the characteristics are approximately rectilinear, Eqs. 24. Therefore, the lattice of characteristics in the x,t-diagram takes the well-known shape of Fig. 16.
Integration of the compatibility equations, Eqs. 25, along the characteristics yields

$$u_j + \frac{1}{\rho_o c_o} p_j = u_{j-1} + \frac{1}{\rho_o c_o} p_{j-1} - \frac{\lambda}{2D} u_{j-1} |u_{j-1}| \Delta t + O(\Delta t^2)$$

$$u_j - \frac{1}{\rho_o c_o} p_j = u_{j+1} - \frac{1}{\rho_o c_o} p_{j+1} - \frac{\lambda}{2D} u_{j+1} |u_{j+1}| \Delta t + O(\Delta t^2)$$

in which subscript j indicates the lattice point and Δt represents the time step. Neglecting the terms $O(\Delta t^2)$, these equations can be solved for the two unknowns u_j and p_j at the new time step. When pressures and velocities on a row are known, the procedure is applied to the next row, etc.
The boundary conditions at the ends of a row are given either by one of the conditions at x = o (pump) and x = 1 (reservoir) or by a shock relation, Eq. 47.

Initial curve and initial conditions of the cavitation region

When the first point in which the pressure is lower than the vapor pressure is detected during the water hammer computation, the registration of the position of the initial curve and the calculation of the initial conditions of the cavitation region is started, and is continued during the computation of the following rows. A problem which arises, is to find the moment that the initial curve ceases to exist and the shock starts to develop.
To solve this problem a continuous transition between water hammer and cavitation regions is considered, and the celerity of the transition is supposed to be less than the celerity c_o, see Fig. 17. Points 1 and 3 are situated on the transition, point 2 is situated in the water hammer region, point 4 in the cavitation region.

Directions 1 - 2 and 2 - 3 are characteristic directions in the water hammer region, 1 - 4 is the characteristic direction in the cavitation region. As the four points are close to each other, friction influences may be neglected. Eqs. 25 and 32 yield

$$u_2 + \frac{1}{\rho_o c_o} p_2 = u_1 + \frac{1}{\rho_o c_o} p_1$$

$$u_3 - \frac{1}{\rho_o c_o} p_3 = u_2 - \frac{1}{\rho_o c_o} p_2$$

$$u_1 = u_4$$

in which $p_1 = p_3 = p_v$

Eliminating u_2 and u_1, one obtains

$$u_4 - u_3 = \frac{2}{\rho_o c_o} (p_2 - p_v)$$

The right member of this equation is positive, because the pressure in the water hammer region is always above vapor pressure. Hence

$$u_4 > u_3$$

This means that a shock would develop. However, the above reasoning is only valid if point 3 can be influenced by point 1, or, in other words, if the celerity of the continuous transition is less than the celerity c_o. In this way one finds that, if

$$|c_i| = \left|\frac{dx_i}{dt_i}\right| > c_o$$

the transition is continuous, and a shock starts to develop as soon as $|c_i|$ becomes less than c_o.

The shape of the initial curve is approximated by the lattice points in which the pressure falls below the vapor pressure and cavitation starts,

see Fig. 18. As the celerity of the initial curve is greater than the water hammer celerity, boundary conditions for the water hammer computation are not needed on this curve.
The solution of the equations for the cavitation region is given by Eqs. 31, 37 and 38. Equations 37 and 38 may be simplified, again making use of the fact that the flow velocity is much less than the celerity:

$$\frac{u_o}{c_o} << 1$$

The results are for the vapor concentration

$$k \approx \left[\frac{du_i}{dx_i} + \frac{\lambda}{2\,D} \frac{u_i |u_i|}{\frac{dx_i}{dt_i}} \right] \cdot \frac{t - t_i}{1 + \frac{\lambda}{2\,D} |u_i| \, (t - t_i)}$$

and for the characteristics

$$x - x_i \approx o$$

In the equation for the concentration k, expressions are required for the quantities $\frac{du_i}{dx_i}$ and $\frac{dx_i}{dt_i}$, which cannot be computed with some degree of accuracy from the crude approximation of the initial curve.
Therefore, these derivatives are replaced by derivatives of quantities in the adjacent water hammer region.
On the initial curve the condition

$$dp = o$$

or

$$\left(\frac{\partial p}{\partial x}\right)_i dx_i + \left(\frac{\partial p}{\partial t}\right)_i dt_i = o$$

holds.
Derivatives with respect to t are unconvenient in the numerical scheme and therefore, the equation of continuity, Eq. 22, is used to eliminate $\left(\frac{\partial p}{\partial t}\right)_i$.
The result is

$$\frac{dx_i}{dt_i} = c_i = \rho_o c_o^2 \frac{\left(\frac{\partial u}{\partial x}\right)_i}{\left(\frac{\partial p}{\partial x}\right)_i}$$

in which

$$\left(\frac{\partial u}{\partial x}\right)_i \approx \frac{u_{j+2} - u_j}{\Delta x} \text{ and } \frac{\partial p}{\partial x}_i \approx \frac{p_{j+2} - p_j}{\Delta x}$$

The lattice points j and j + 2 are situated in the water hammer region, and nearest to the initial curve.
An expression for $\frac{du_i}{dx_i}$ is derived in a similar way.
The total differential of the velocity u on the initial curve reads

$$du_i = \left(\frac{\partial u}{\partial x}\right)_i dx_i + \left(\frac{\partial u}{\partial t}\right)_i \frac{dx_i}{c_i}$$

Again the derivative with respect to t is eliminated, applying the equation of motion, Eq. 23, this time.
The result is

$$\frac{du_i}{dx_i} = \left(\frac{\partial u}{\partial x}\right)_i - \frac{1}{\rho_o c_i}\left(\frac{\partial p}{\partial x}\right)_i - \frac{1}{c_i}\frac{\lambda}{2D} u_i|u_i|$$

or

$$\frac{du_i}{dx_i} = \left[1 - \frac{c_o^2}{c_i^2}\right]\left(\frac{\partial u}{\partial x}\right)_i - \frac{1}{c_i}\frac{\lambda}{2D} u_i|u_i|$$

With the expressions for $\frac{du_i}{dx_i}$ and $\frac{dx_i}{dt_i}$ the equation for the concentration k changes to

$$k = \left[1 - \frac{c_o^2}{c_i^2}\right] \frac{\left(\frac{\partial u}{\partial x}\right)_i (t - t_i)}{1 + \frac{\lambda}{2D}|u_i|\,(t - t_i)}$$

The vapor concentration k in the cavitation region is not less than zero.
Consequently

$$\left[1 - \frac{c_o^2}{c_i^2}\right] \left(\frac{\partial u}{\partial x}\right)_i \geq o$$

The equation for c_i gives

$$\left(\frac{\partial u}{\partial x}\right)_i = \frac{1}{\rho_o c_o^2} c_i \left(\frac{\partial p}{\partial x}\right)_i$$

The pressure in the water hammer region is not less than the pressure in the cavitation region. Therefore, it is easily seen that, if $c_i > o$ then $\left(\frac{\partial p}{\partial x}\right)_i \geq o$, and if $c_i < o$ then $\left(\frac{\partial p}{\partial x}\right)_i \leq o$. Thus $\left(\frac{\partial u}{\partial x}\right)_i$ is found to be not less than zero.
With this result the above inequality changes to

$$1 - \frac{c_o^2}{c_i^2} \geq o$$

or

$$|c_i| \geq c_o$$

which is consistent with the earlier results, derived from the shock conditions.

As the derivatives of pressure and velocity have to be determined numerically, the prescribed pressure drop at $x = o$ should have a smooth course.
The quantities x_i, t_i, u_i, c_i and $\left(\frac{\partial u}{\partial x}\right)_i$ are computed in all lattice points of the approximated initial curve and stored in view of the calculation of the shocks in a later phase of the computation.
If $|c_i| < c_o$ and $\left(\frac{\partial u}{\partial x}\right)_i < o$, which occurs close to the point where the shock starts, these values are replaced by the values in the preceding initial curve point and the computation of the part of the initial curve considered is terminated.

Some time after closure of the first cavitation region a second caviation region may develop, which generally has a more irregular shape than the first one. It appeared necessary to adapt the program to the occurence of initial curves with inflexion points.

Computation of shock waves

The propagation of a shock wave during a time step Δt is computed making use of a modified Euler scheme. The predictor is

$$x_s(t + \Delta t) = x_s(t) \pm c_s(t) \cdot \Delta t$$

The initial values $x_s(t)$ and $c_s(t)$ are assumed to be known from the computation of the preceding row.
The computation starts in the lattice point in which the initial curve ceases to exist. The shock celerity c_s in this point is unknown, but satisfies the inequality

$$o < c_s < c_o$$

Some test runs showed that the shock computation converged to the same solution for different values of the celerity c_s in the starting point. However, in one case the shock appeared to start too fast, which caused pressures below vapor pressure in the water hammer region. Therefore,

$$c_s = o$$

was chosen as the starting value in the computation.
At the new position of the shock, $x = x_s(t + \Delta t)$, the velocity u_v and vapor concentration k in the cavitation region are computed. Eqs. 46 and 47 for the shock and a compatibility equation along characteristic (a) in Fig. 19a yield the new shock celerity c_s, pressure p_f and velocity u_f.
In the compatibility equation the velocity and pressure in point A are replaced by the values in the lattice point B, as linear interpolation between points C and B yielded unrealistic results.
The corrector

$$x_s(t + \Delta t) = x_s(t) \pm \frac{1}{2} \left[c_s(t + \Delta t) + c_s(t)\right] \Delta t$$

gives the final position of the shock at the new time step. Velocity, pressure and celerity at the new time step are not corrected.
If point D lies inside the water hammer region the velocity and pressure

in this point are taken equal to the values at the new position of the shock (point E).
When the two shock paths intersect the shock computation is terminated and the resulting pressure and velocity in the closest lattice point at the new time step follow from the water hammer equations along characteristics (b) and (c) in Fig. 19b. Sometimes two lattice prints have to be considered as one point (F), Fig. 19c.
In view of a possible future cavitation region the two sharp pressure fronts, caused by the meeting of the shocks, are spread over some lattice points.
On the boundaries of the second and following caviation regions a shock wave may be removed by a negative pressure wave. After this, again a partial initial curve develops, starting at the point where the shock ceases to exist. The program takes this possibility into account.

APPENDIX 2 - References

1. Bergeron, L., Du Coup de Bélier en Hydraulique et du Coup de Foudre en Electricité, Dunod, Paris, 1950.

2. Brown, R.J., "water Column Separation at Two Pumping Plants", Transactions of the ASME, Journal of Basic Engineering, Vol. 90, No. 4, 1968, series D, pp. 521 - 531.

3. Dijkman, H.K.M., and Vreugdenhil, C.B., "The Effect of Dissolved Gas on Cavitation in Horizontal Pipelines", Journal of Hydraulic Research, Delft, The Netherlands, Vol. 7, No. 3, 1969, pp. 301 - 314.

4. Epstein, P.S., and Plesset, M.S., "On the Stability of Gas Bubbles in a Liquid-Gas Solution", The Journal of Chemical Physics, Vol. 18, No. 11, 1950, pp. 1505 - 1509.

5. de Haller, P., and Bédué, A., "The Break-Away of Water Columns as a Result of Negative Pressure Shocks", Sulzer Technical Review, Winterthur, Switzerland, 1951, No. 4, pp. 18 - 25.

6. Plesset, M.S., "Bubble Dynamics", Report No. 85 - 23, California Institute of Technology.

7. Siemons, J., "The Phenomenon of Cavitation in a Horizontal Pipeline due to a Sudden Pump-Failure", Journal of Hydraulic Research, Delft, The Netherlands, Vol. 5, No. 2, 1967, pp. 135 - 152.

APPENDIX 3 - Notation

A	area of cross-section
C	gas constant
D	diameter
E	bulk modulus of pipe wall material
K	modulus of compressibility of fluid
L	length of pipe-line
N	number of bubbles per unit of mass of fluid
R	radius of bubble
W	friction
a,b	notation for cross-sections
c	velocity of propagation
f	variable compressibility coefficient
k	bubble concentration
n	coefficient accounting for anchorage system
p	pressure
t	time coordinate
u	velocity
x	spacial coordinate
δ	wall thickness
λ	friction parameter
ρ	specific density
σ	surface tension

subscripts:

f	no cavitation
g	gas
i	initial condition of cavitation region
L	low head reservoir
o	undisturbed situation
s	shock
v	cavitation (vapor)

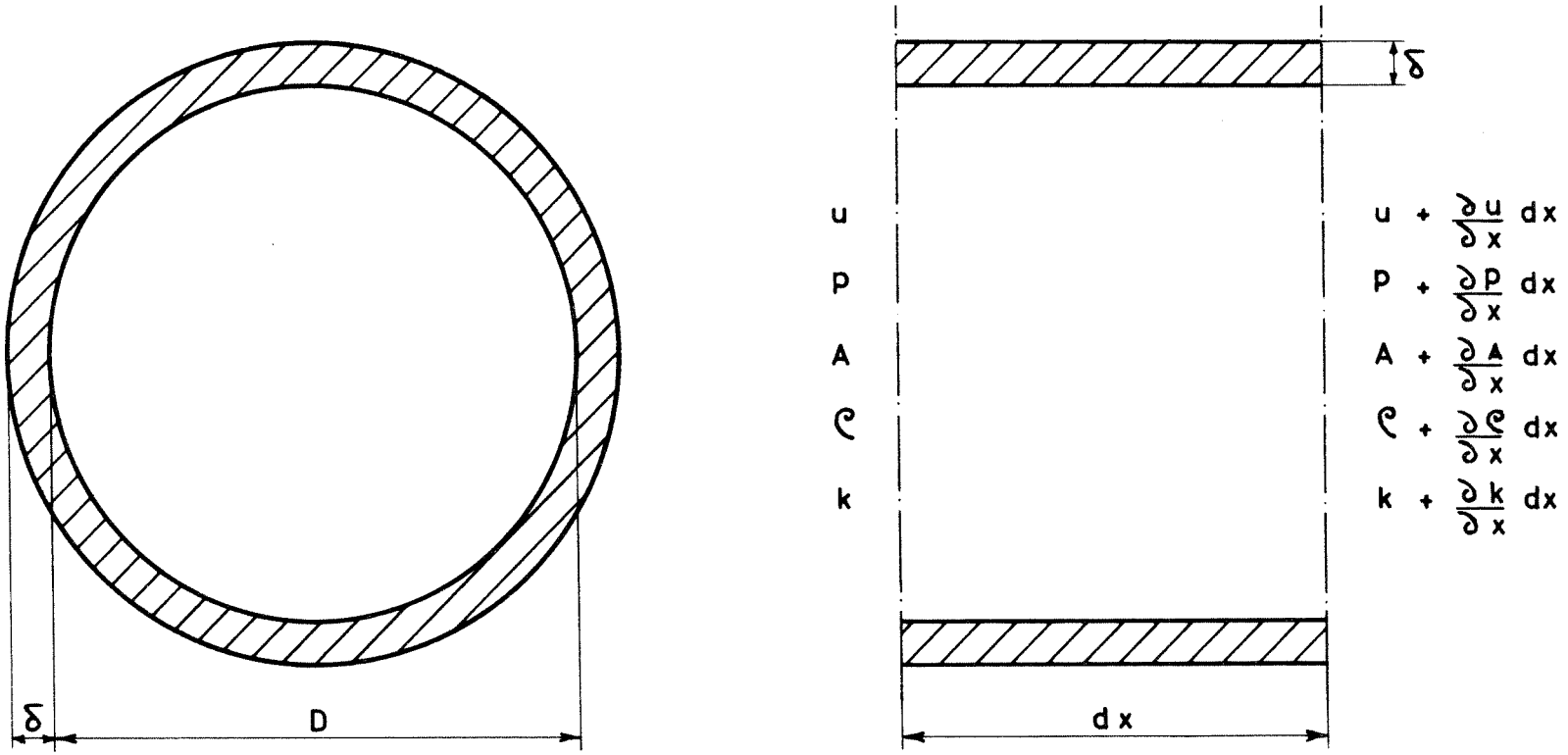

FIG.1-DEFINITION SKETCH

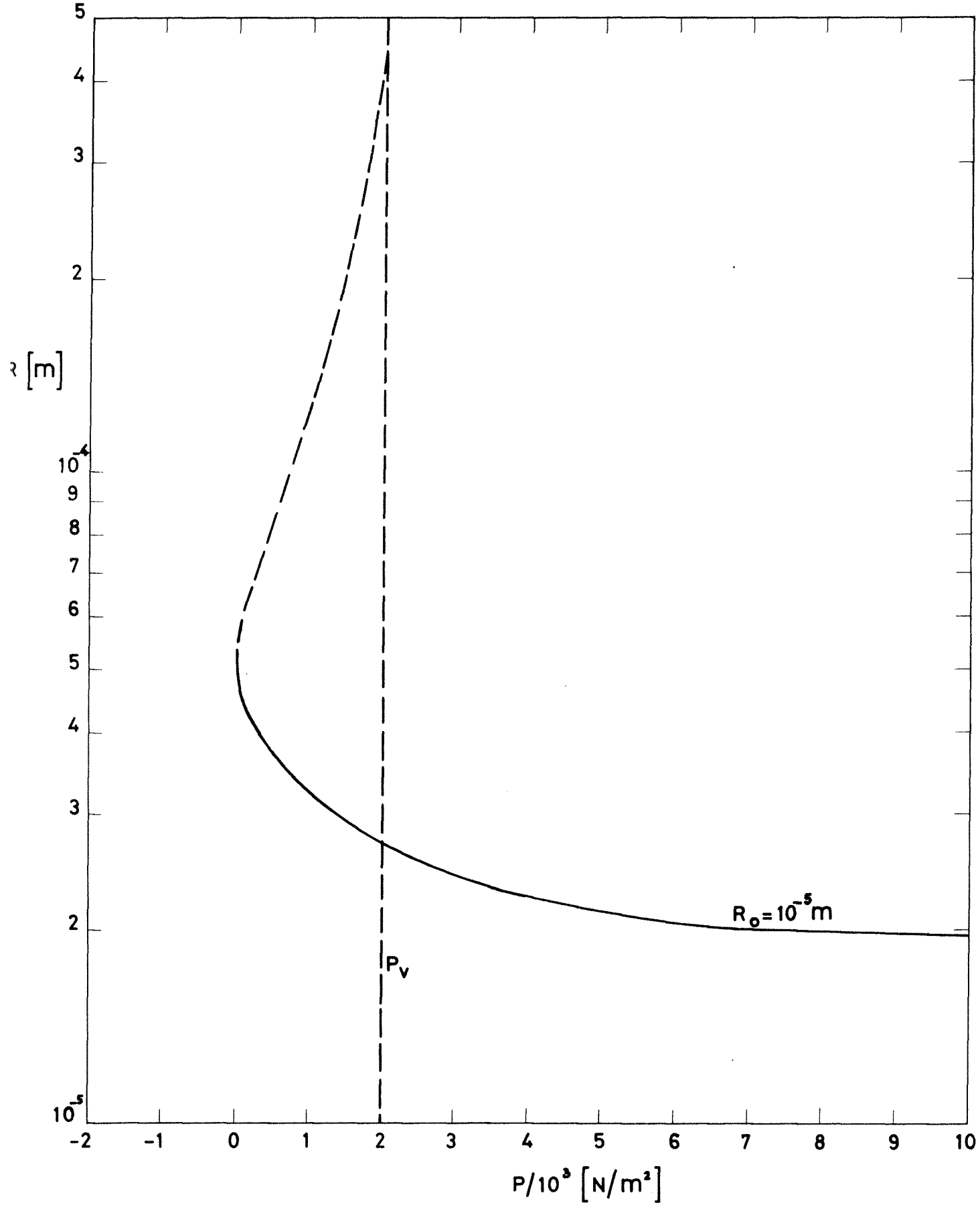

FIG.2-GRAPHICAL REPRESENTATION OF EQUATION [6]

FOR $R_o = 10^{-5}$ m AND $p_o = 10^5$ N/m²

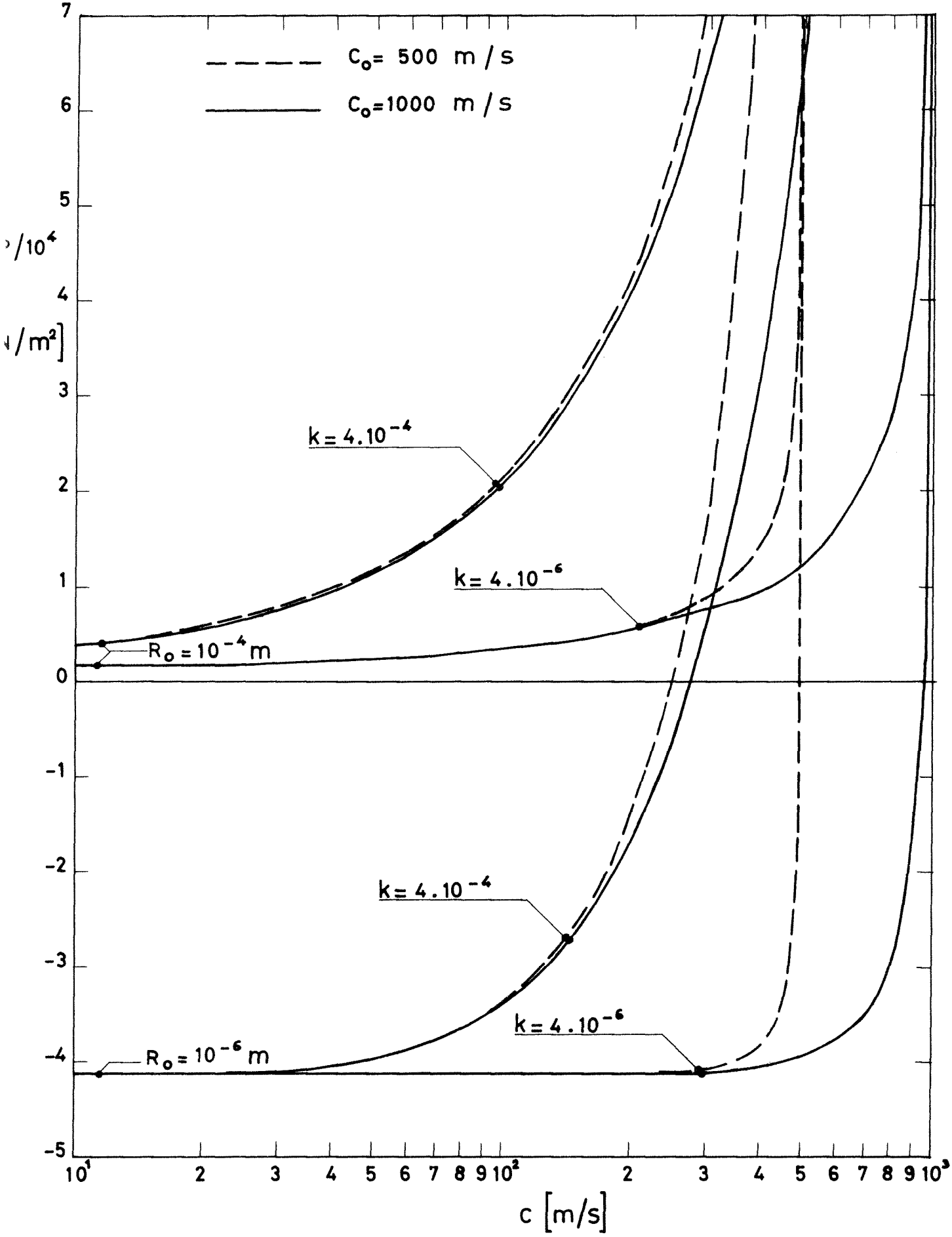

FIG.3–RELATIONSHIP BETWEEN p AND c FOR SOME INITIAL CONDITIONS

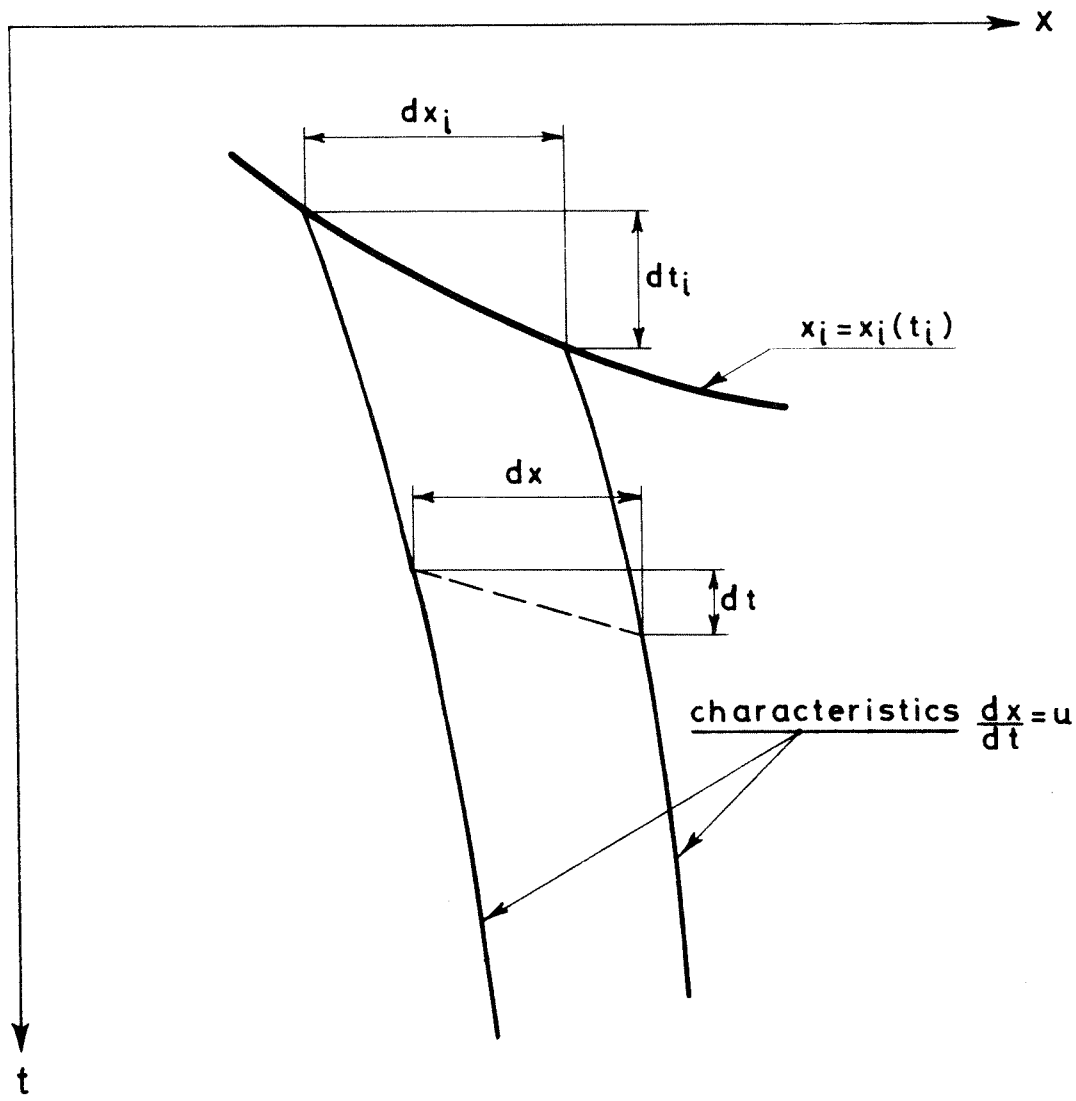

FIG.4–DETERMINATION OF $\frac{\partial u}{\partial x}$

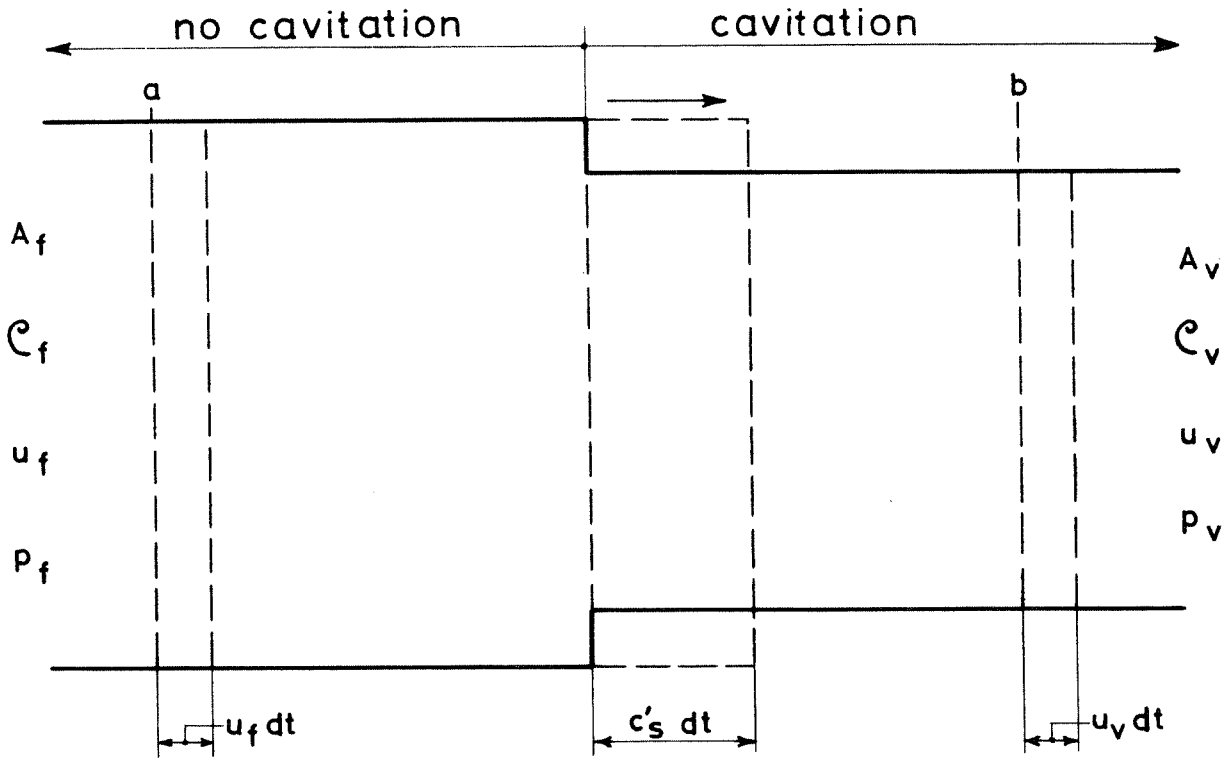

FIG.5-DEFINITION SKETCH OF TRANSITION REGION

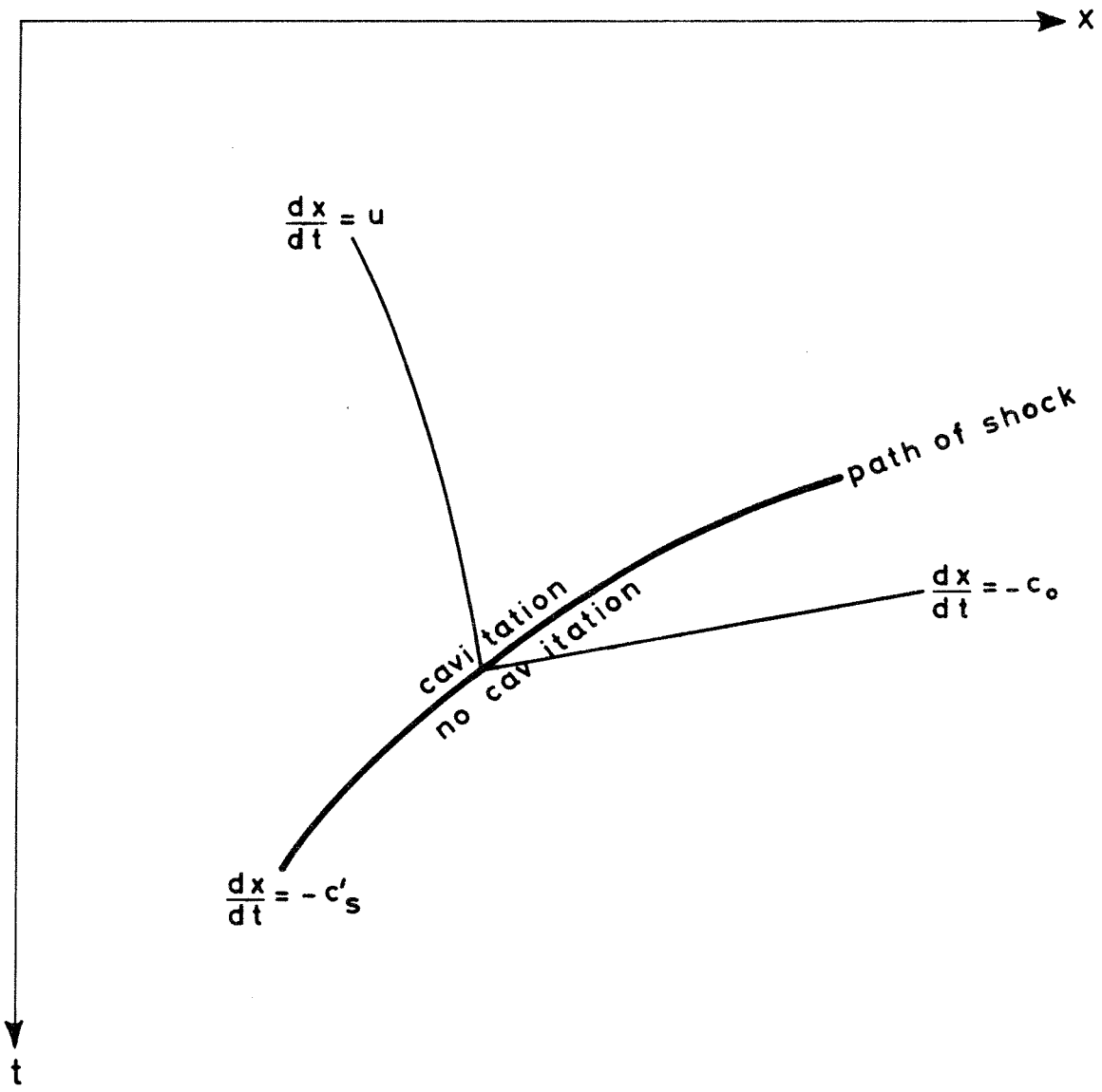

FIG.6-INTERSECTION OF CHARACTERISTICS OF DIFFERENT TYPE

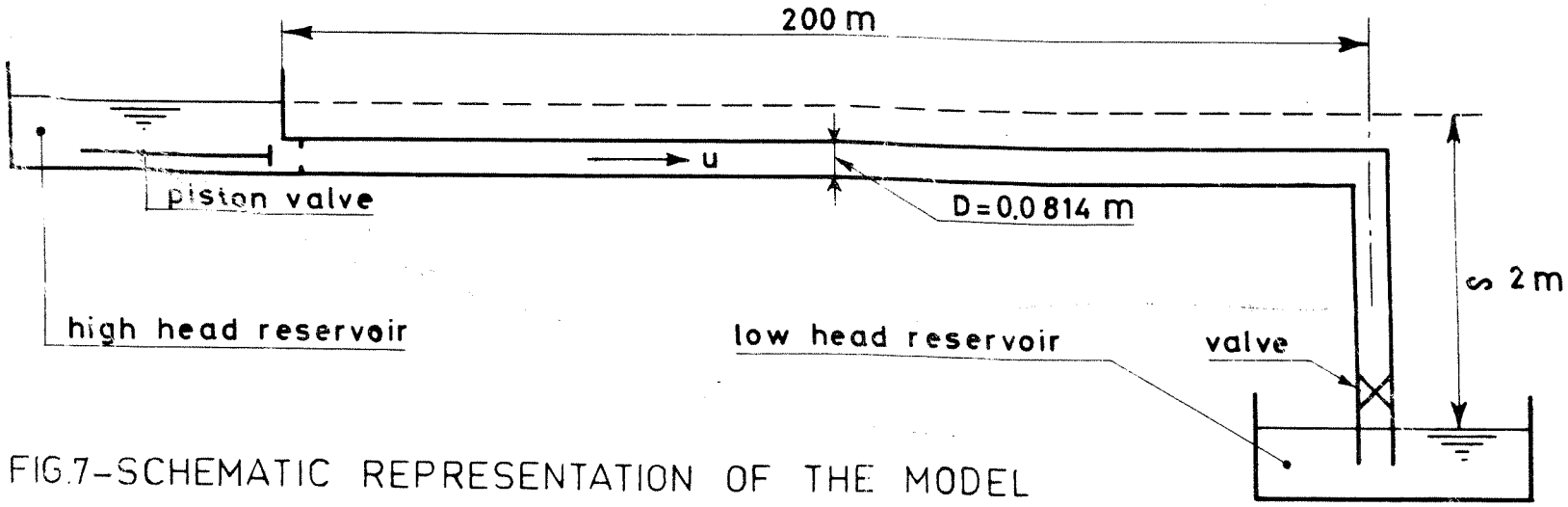

FIG.7–SCHEMATIC REPRESENTATION OF THE MODEL

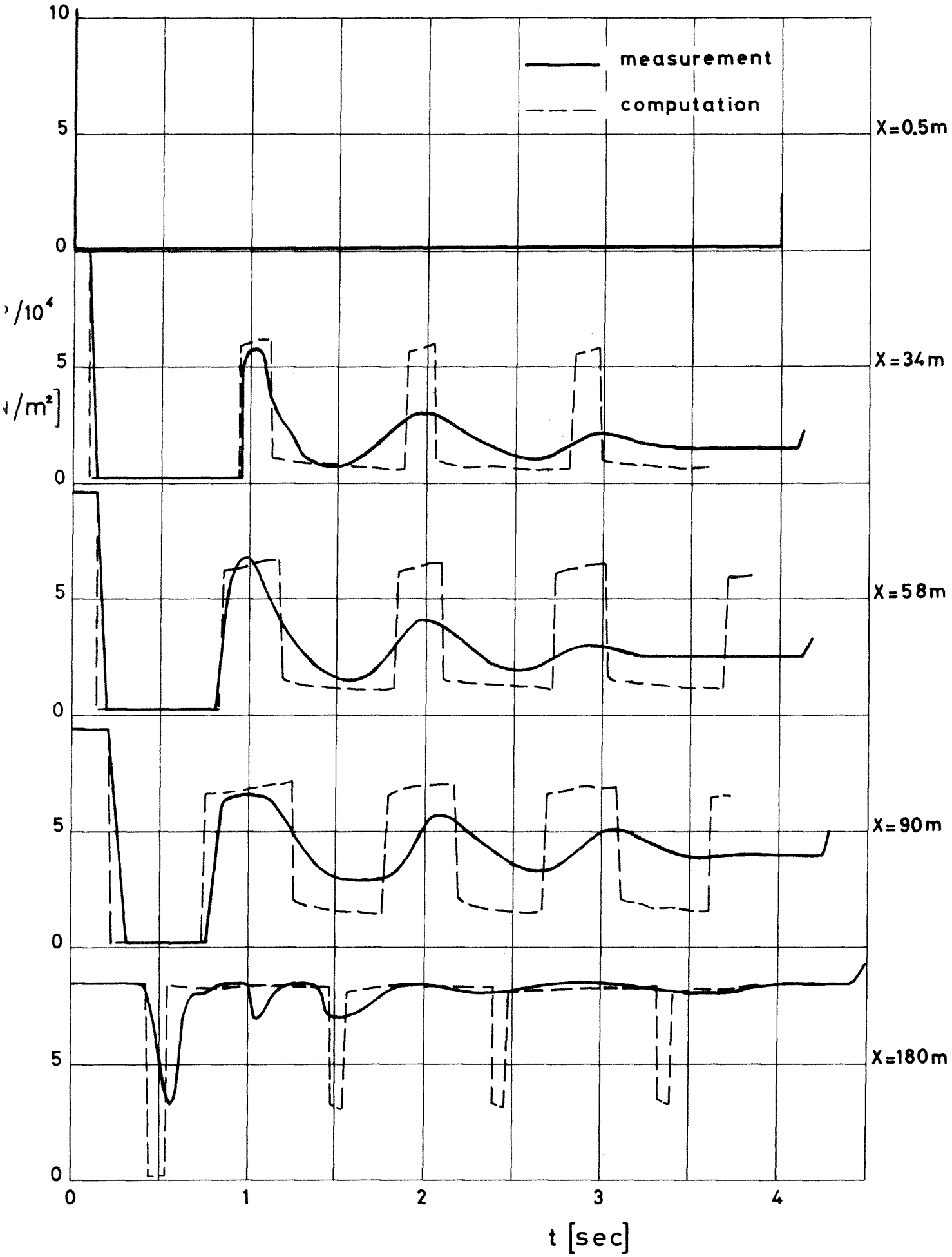

FIG.8-PRESSURE BEHAVIOUR AT SOME LOCATIONS

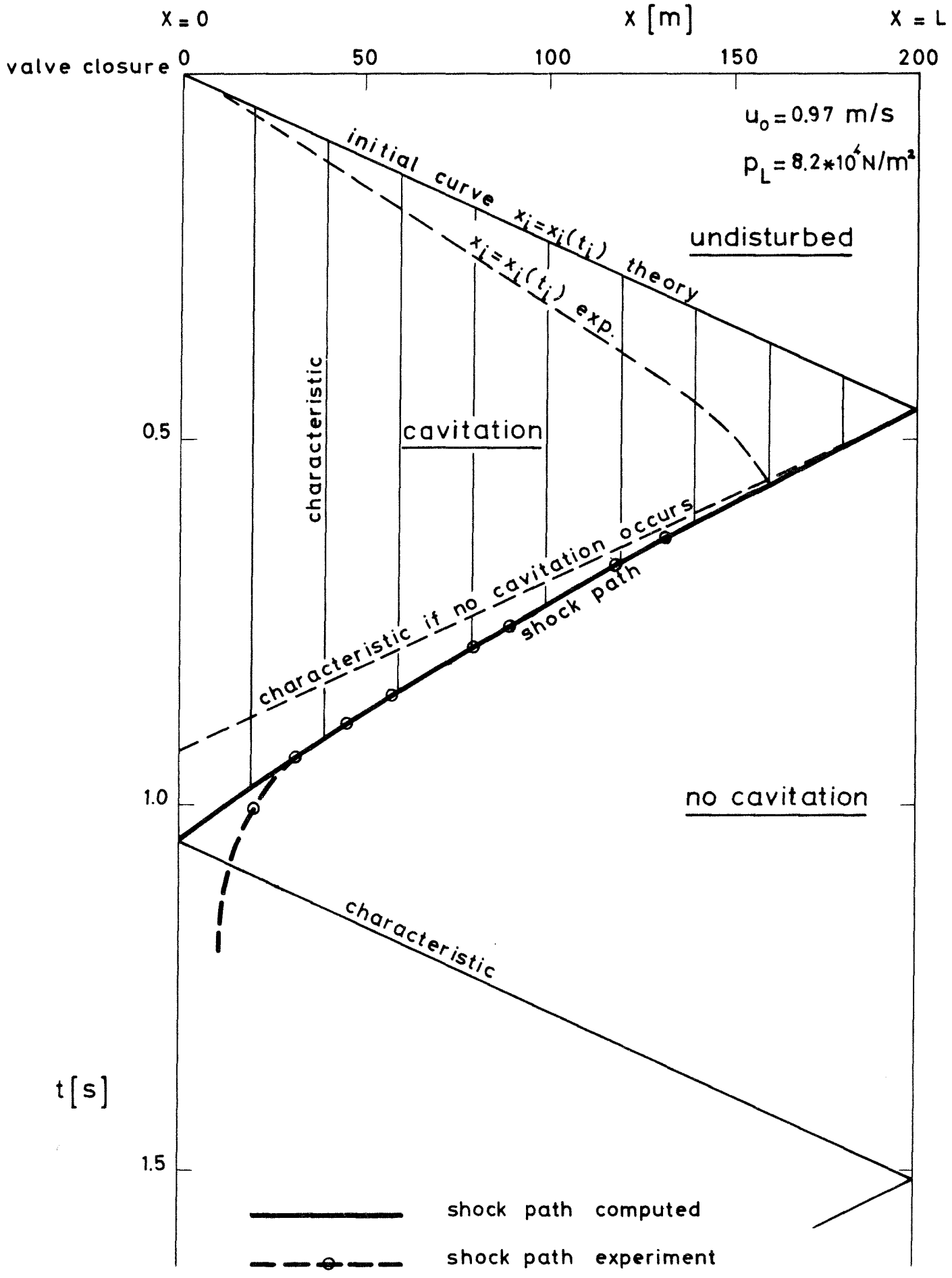

FIG. 9 – x,t DIAGRAM FOR $u_o = 0.97$ m/s AND $p_L = 8.2 * 10^4 N/m^2$

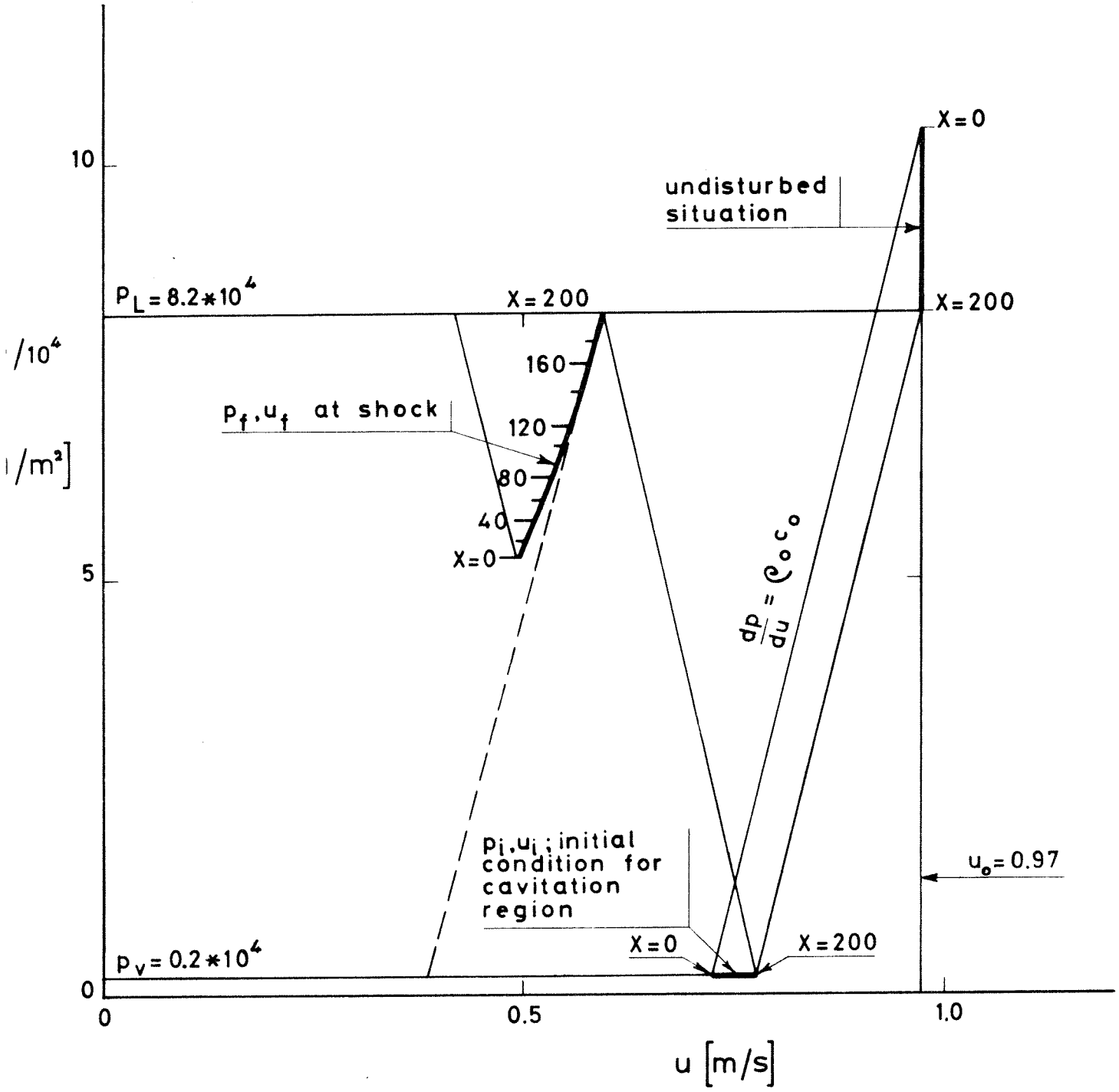

FIG.10-p,u-DIAGRAM (COMPUTATION) FOR

$u_o = 0.97$ m/s AND $p_L = 8.2*10^4$ N/m²

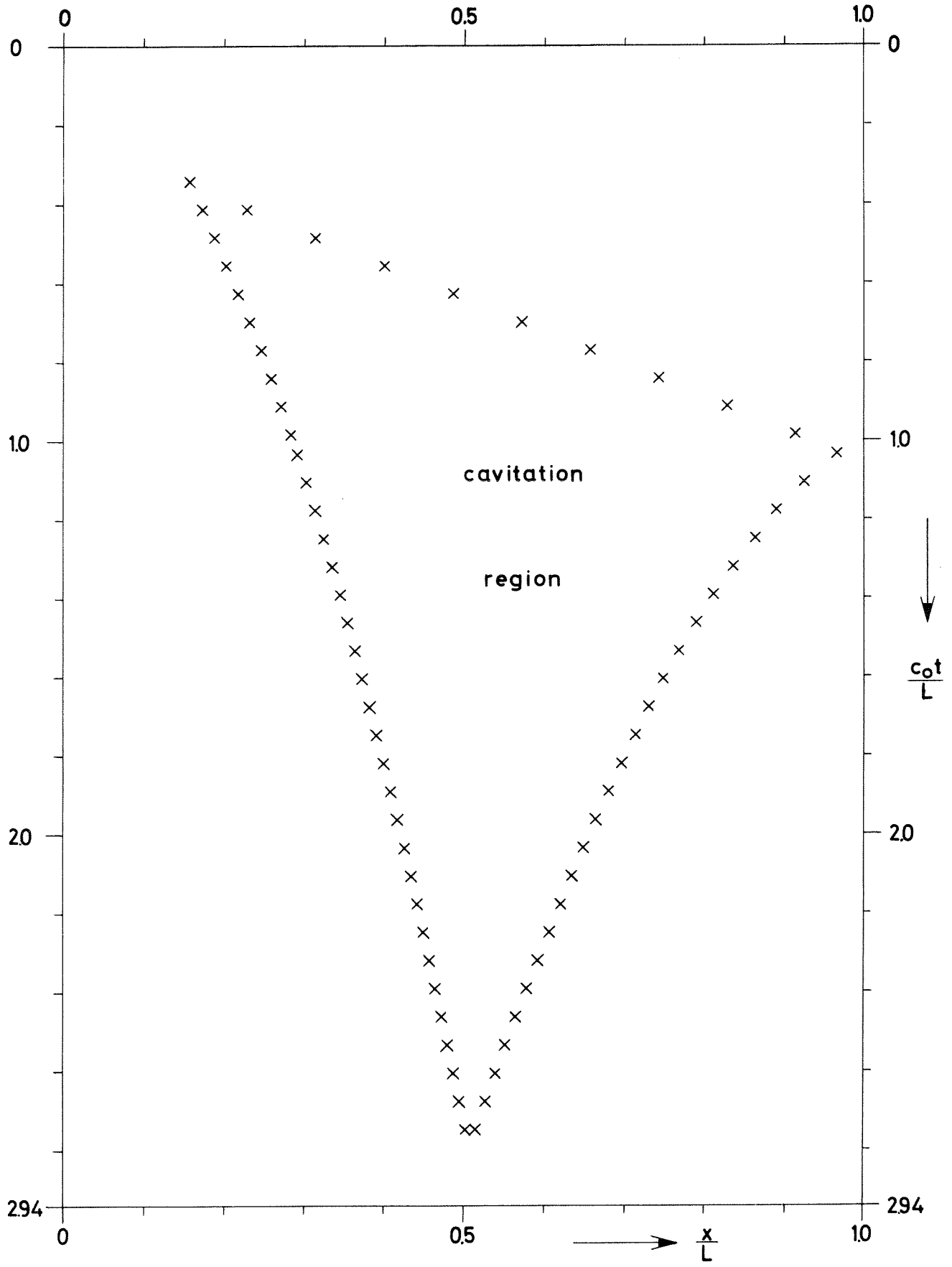

FIG. 11a – x,t DIAGRAM OF CAVITATION REGION, α=0.8, β=0.25, γ=0.2, φ=0.9

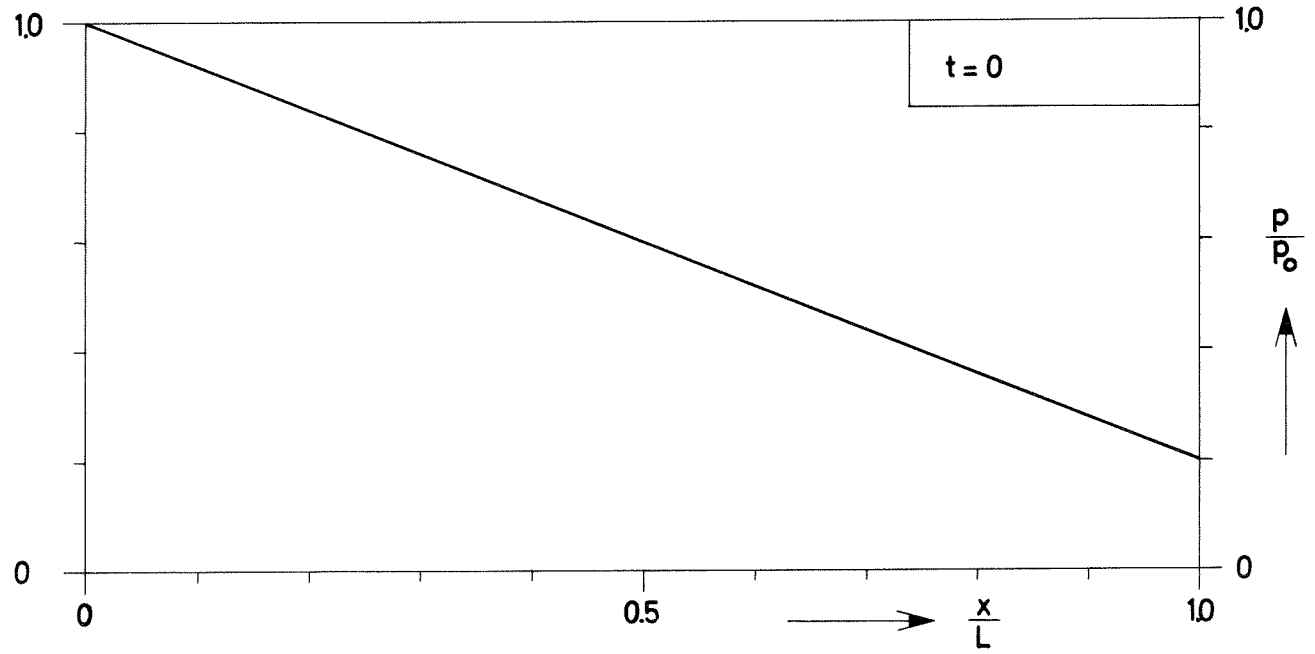

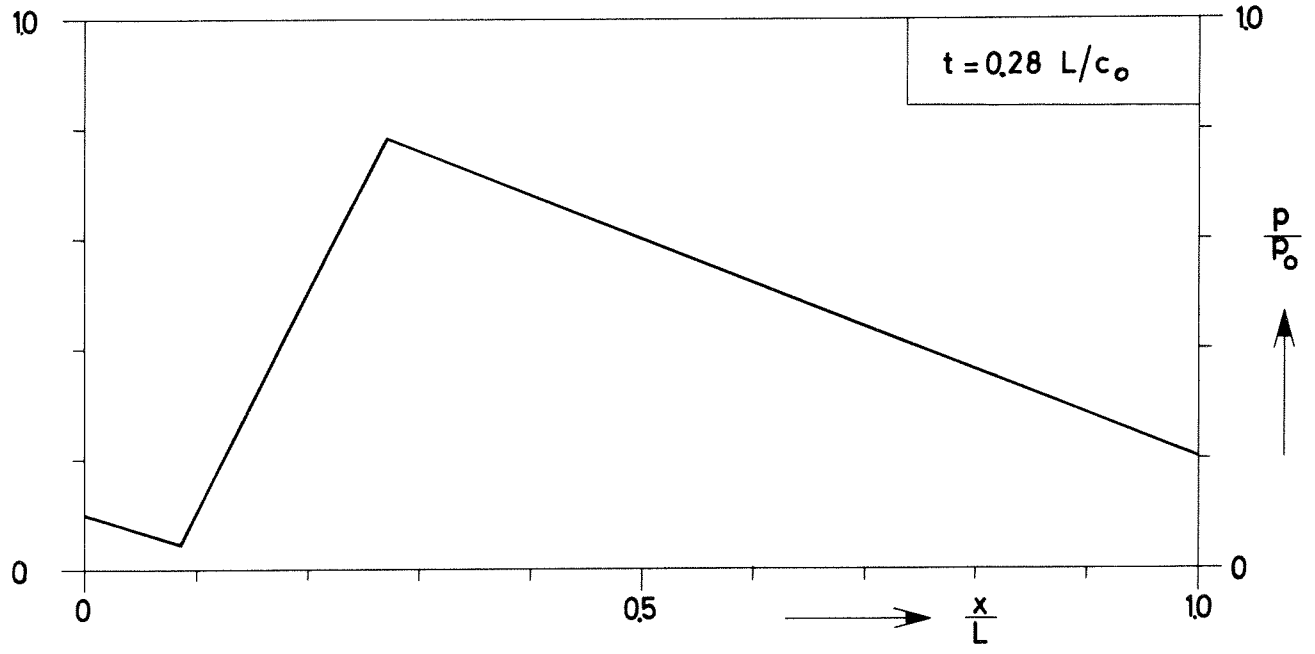

FIG. 11b – p,x DIAGRAMS, $\alpha = 0.8$, $\beta = 0.25$, $\gamma = 0.2$, $\varphi = 0.9$

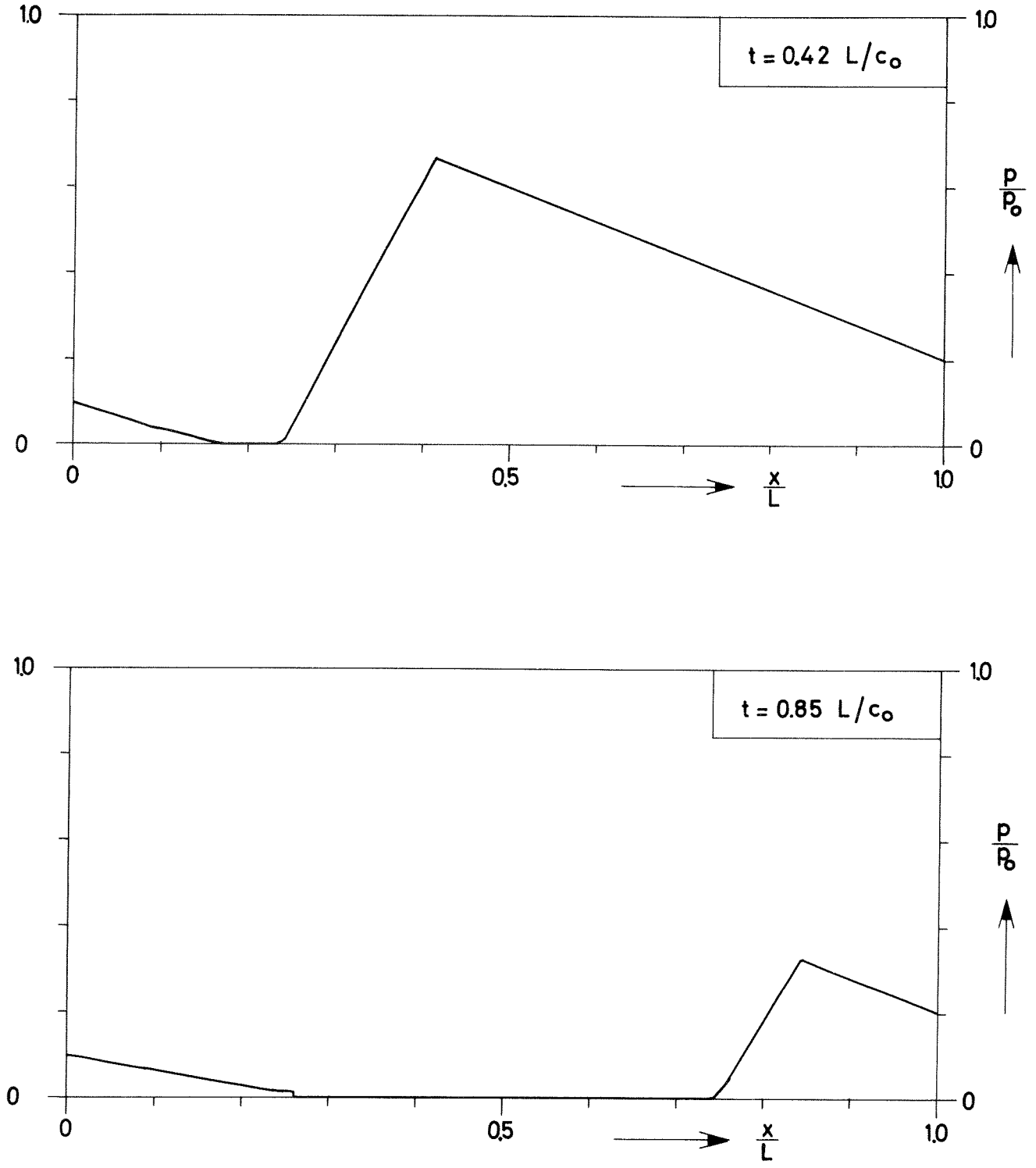

FIG. 11c – p,x DIAGRAMS, $\alpha = 0.8$, $\beta = 0.25$, $\gamma = 0.2$, $\varphi = 0.9$

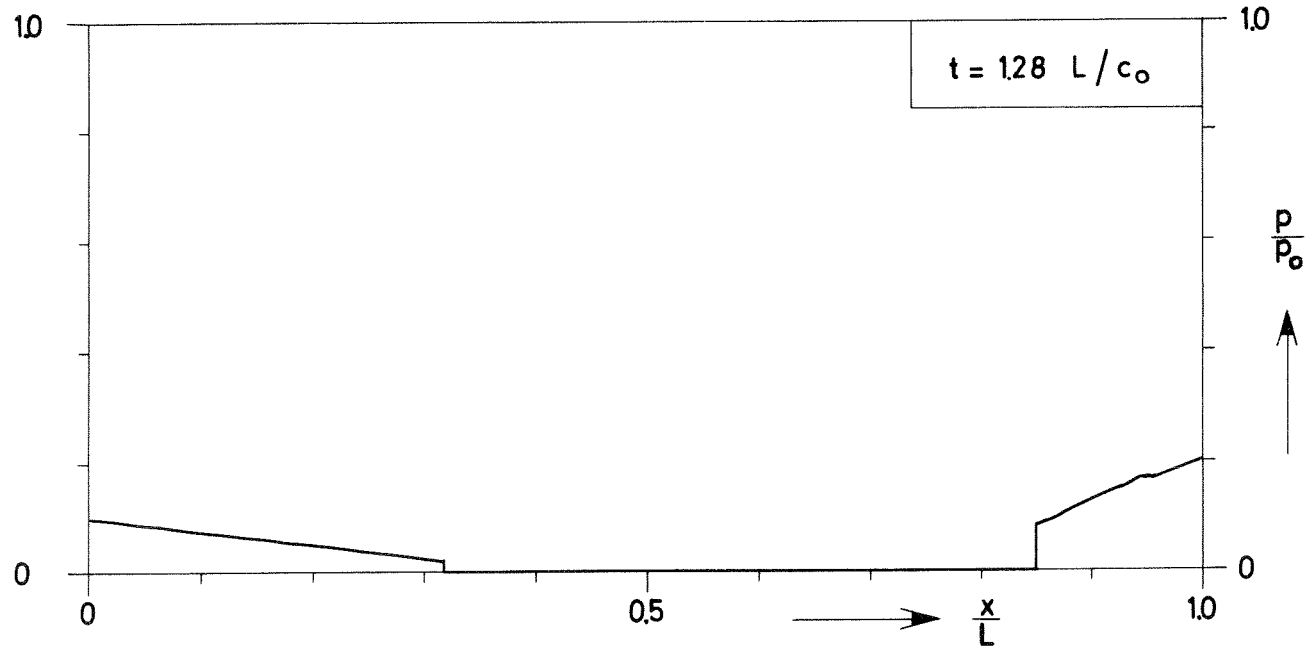

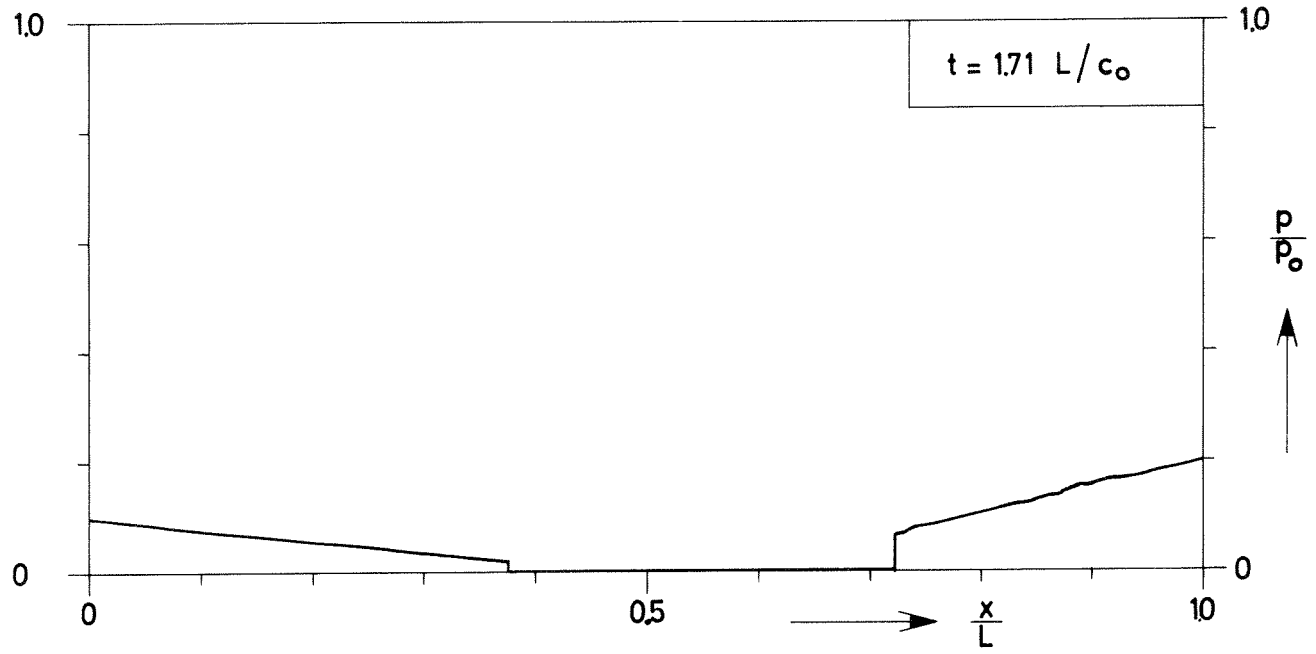

FIG. 11 d–p,x DIAGRAMS, $\alpha = 0.8$, $\beta = 0.25$, $\gamma = 0.2$, $\varphi = 0.9$

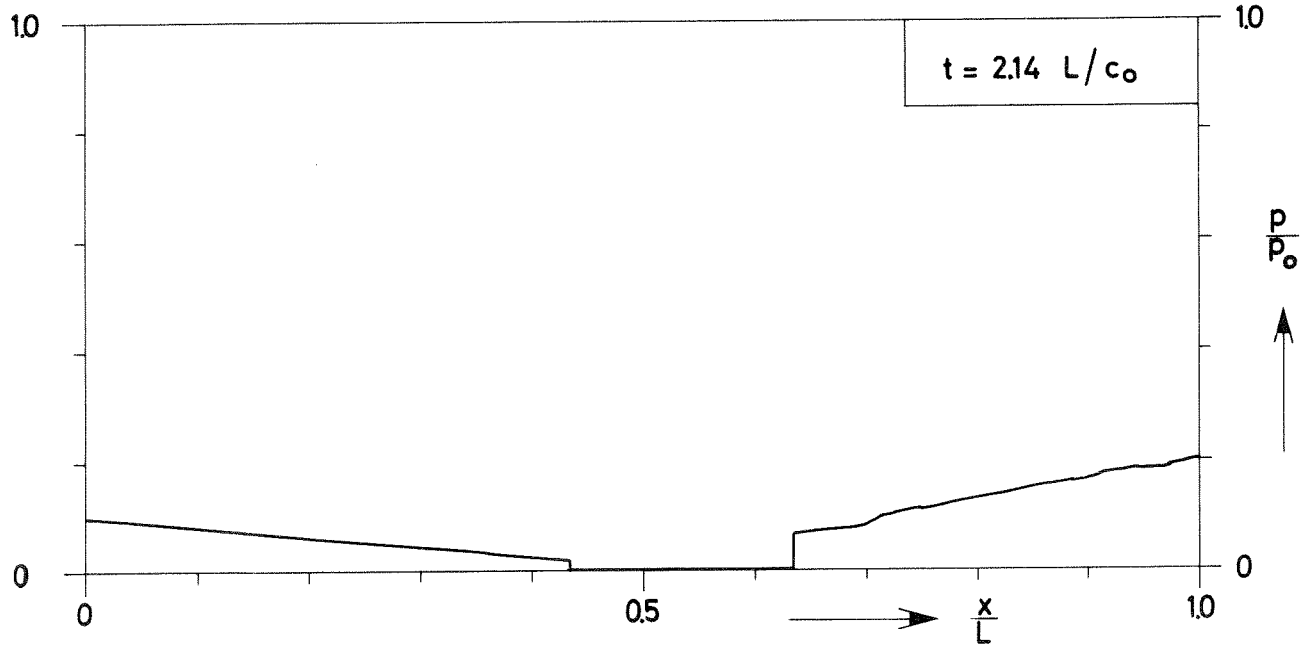

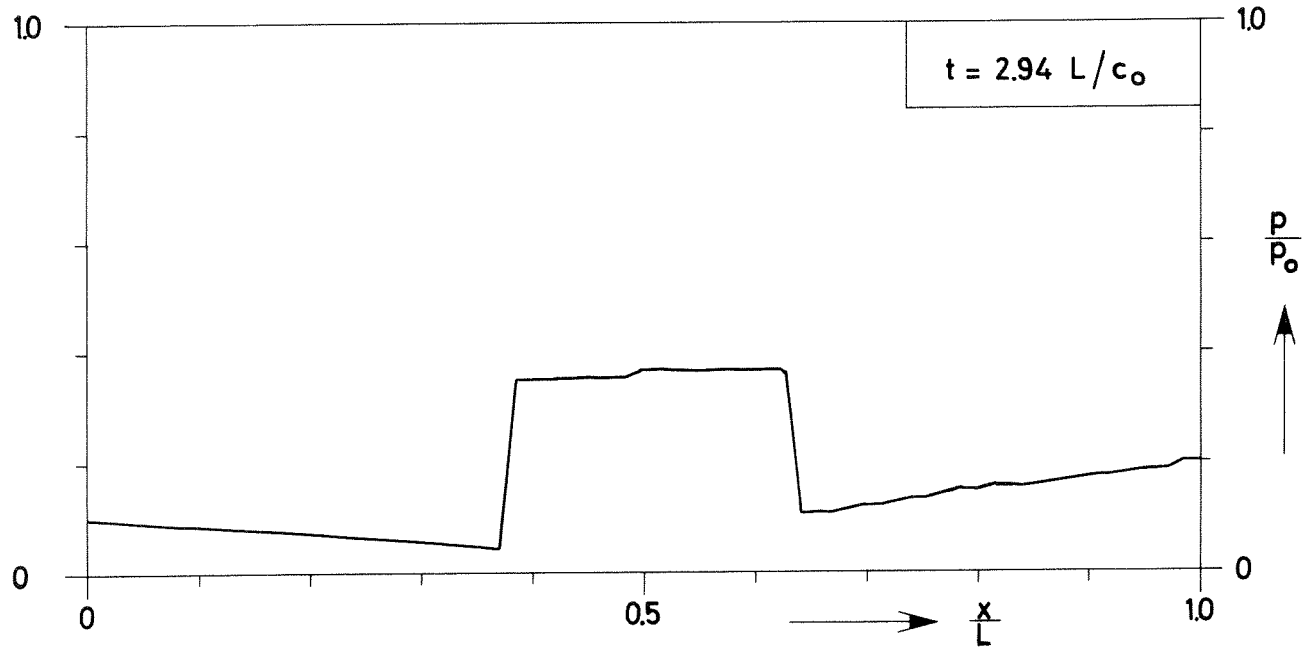

FIG. 11 e - p,x DIAGRAMS, $\alpha = 0.8$, $\beta = 0.25$, $\gamma = 0.2$, $\varphi = 0.9$

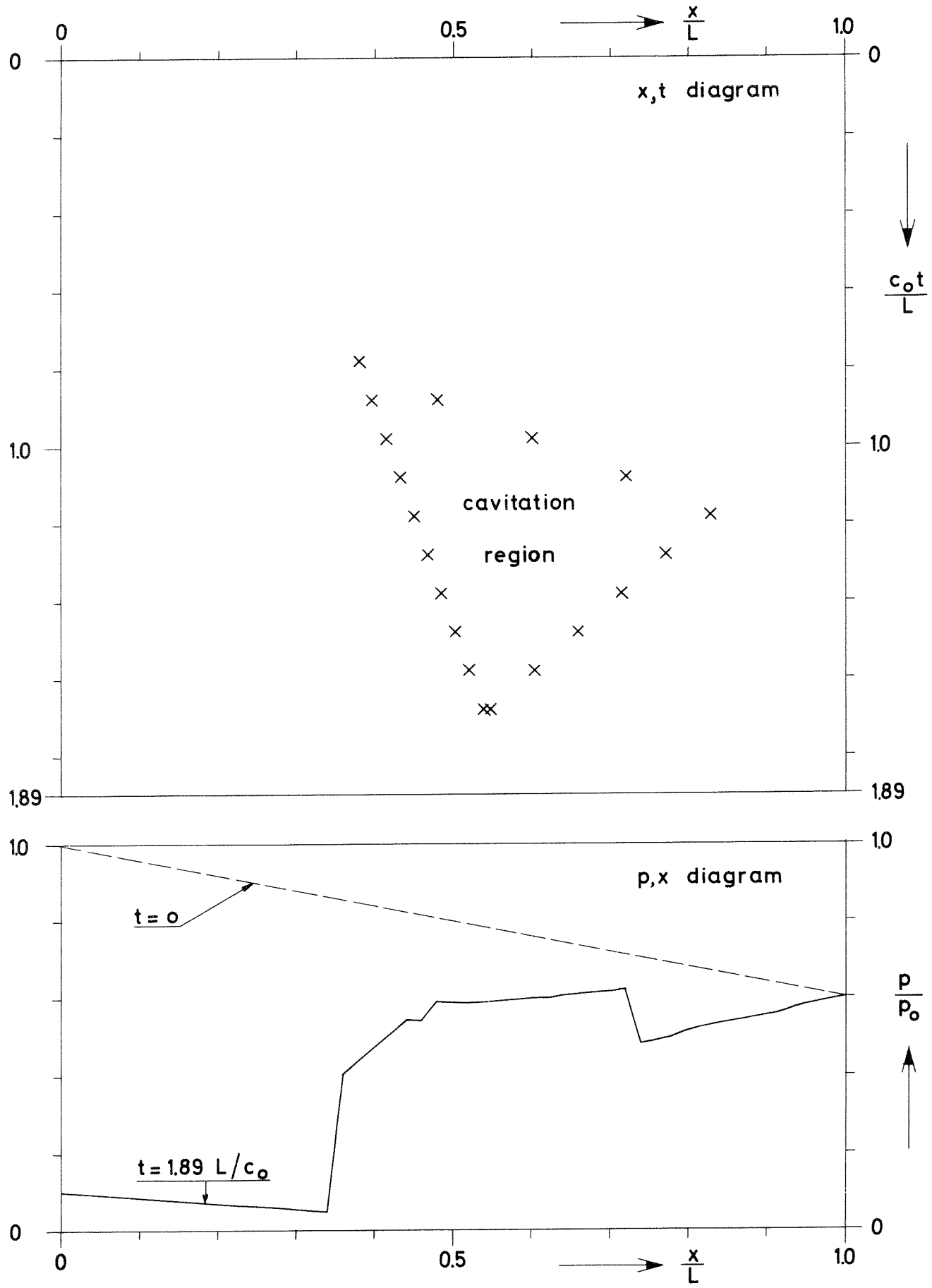

FIG.12a – x,t DIAGRAM AND p,x DIAGRAM AT $0.2\,L/c_o$ AFTER CLOSURE OF CAVITATION REGION, $\alpha = 0.4$, $\beta = 0.5$, $\gamma = 0.4$, $\varphi = 0.9$

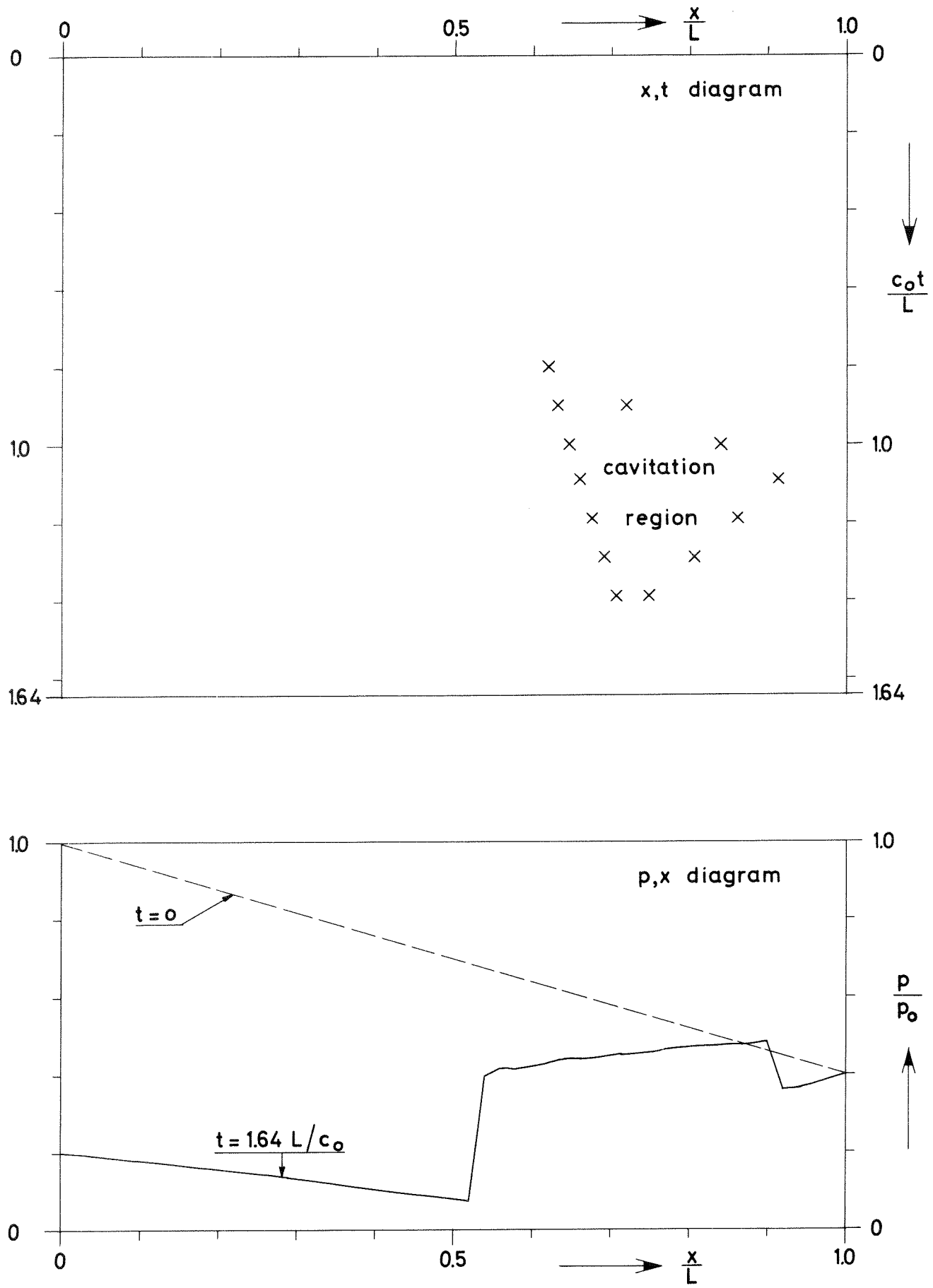

FIG.12b – x,t DIAGRAM AND p,x DIAGRAM AT 0.2 L/c_o AFTER CLOSURE OF CAVITATION REGION, $\alpha = 0.6$, $\beta = 1.0$, $\gamma = 0.2$, $\varphi = 0.8$

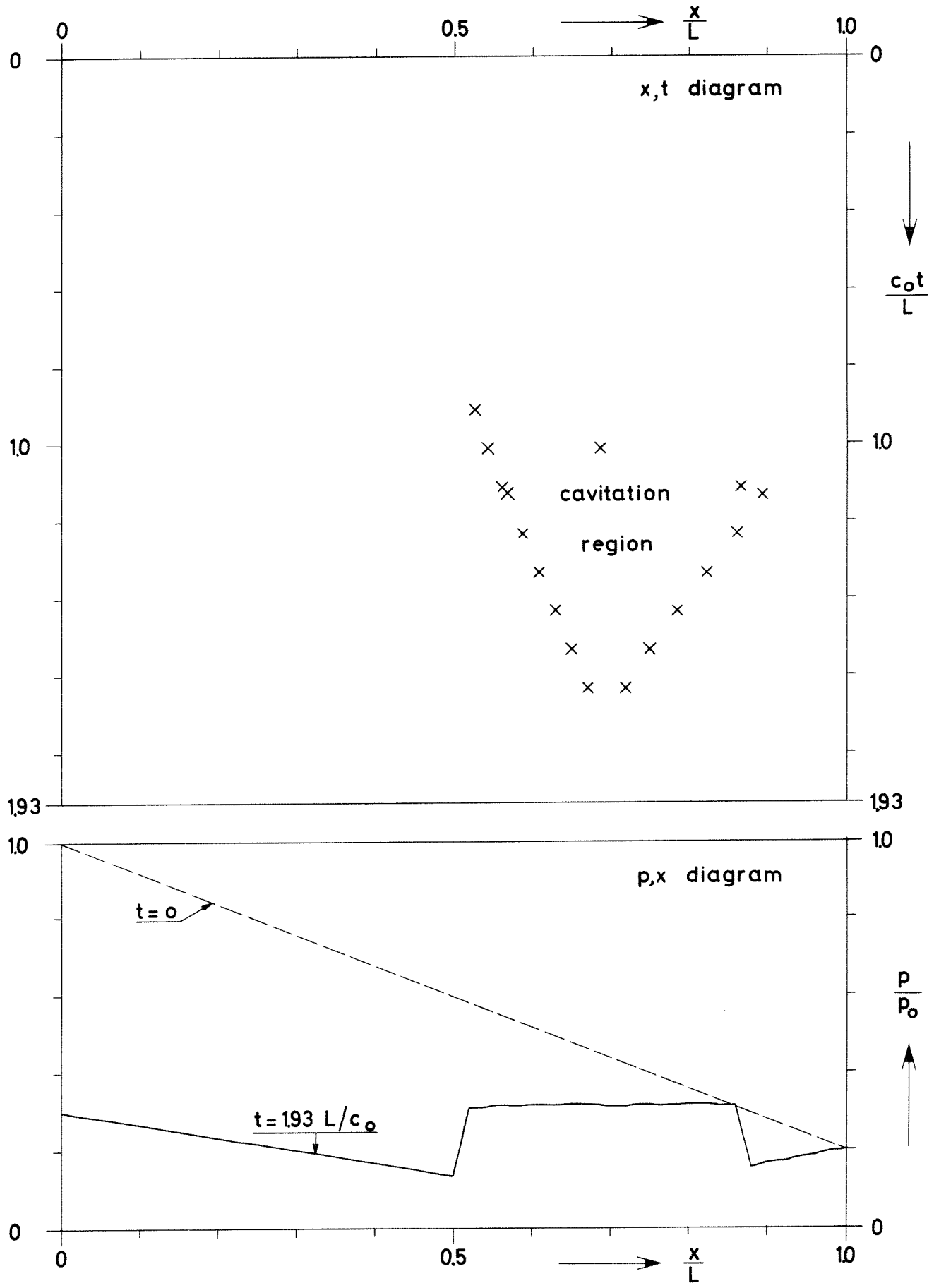

FIG. 12c – x,t DIAGRAM AND p,x DIAGRAM AT 0.2 L/c_o AFTER CLOSURE OF CAVITATION REGION, $\alpha = 0.8$, $\beta = 0.5$, $\gamma = 0.4$, $\varphi = 0.7$

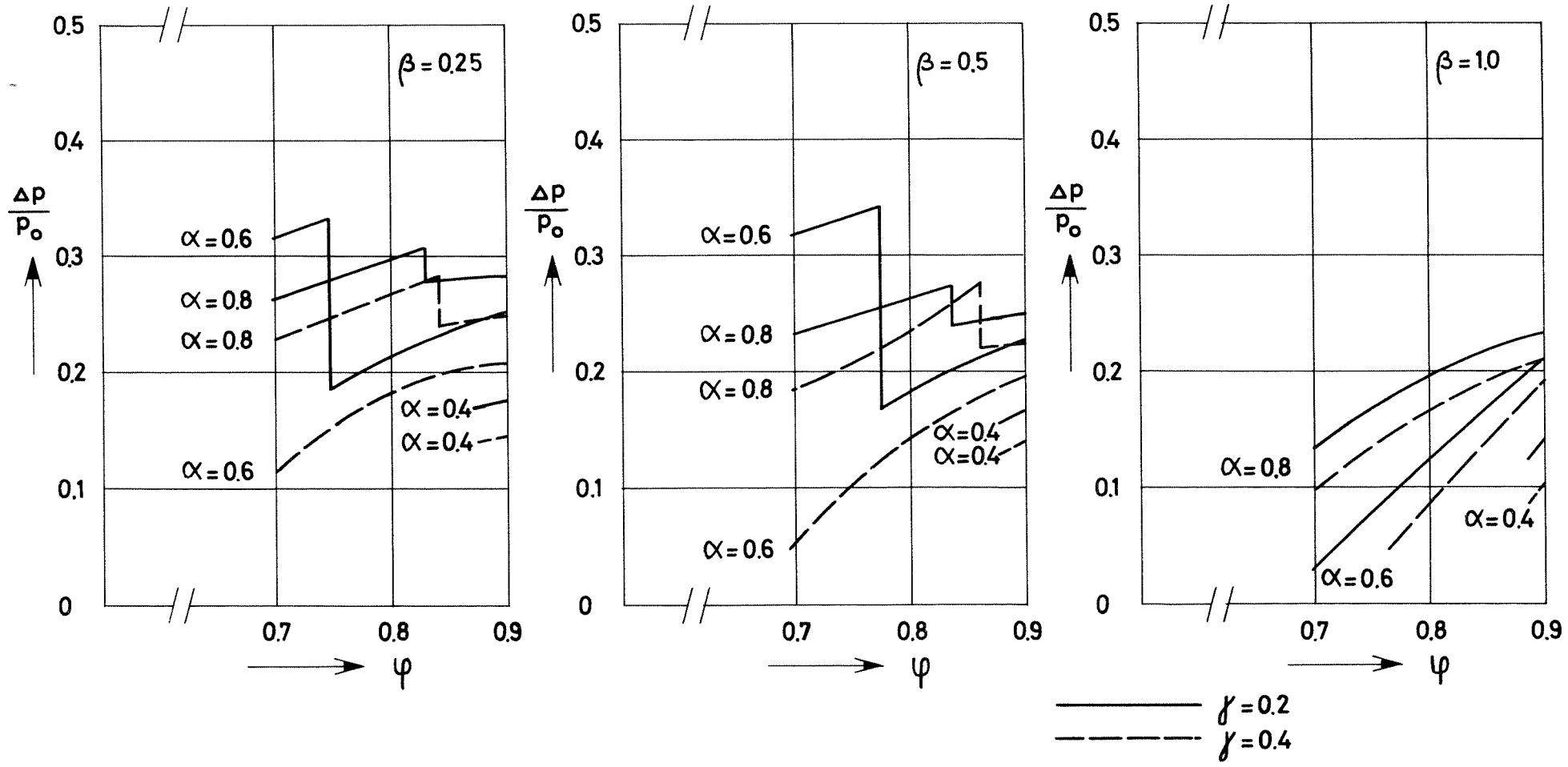

FIG. 13 – MAGNITUDE OF PRESSURE WAVES OCCURRING AFTER CLOSURE OF CAVITATION REGION

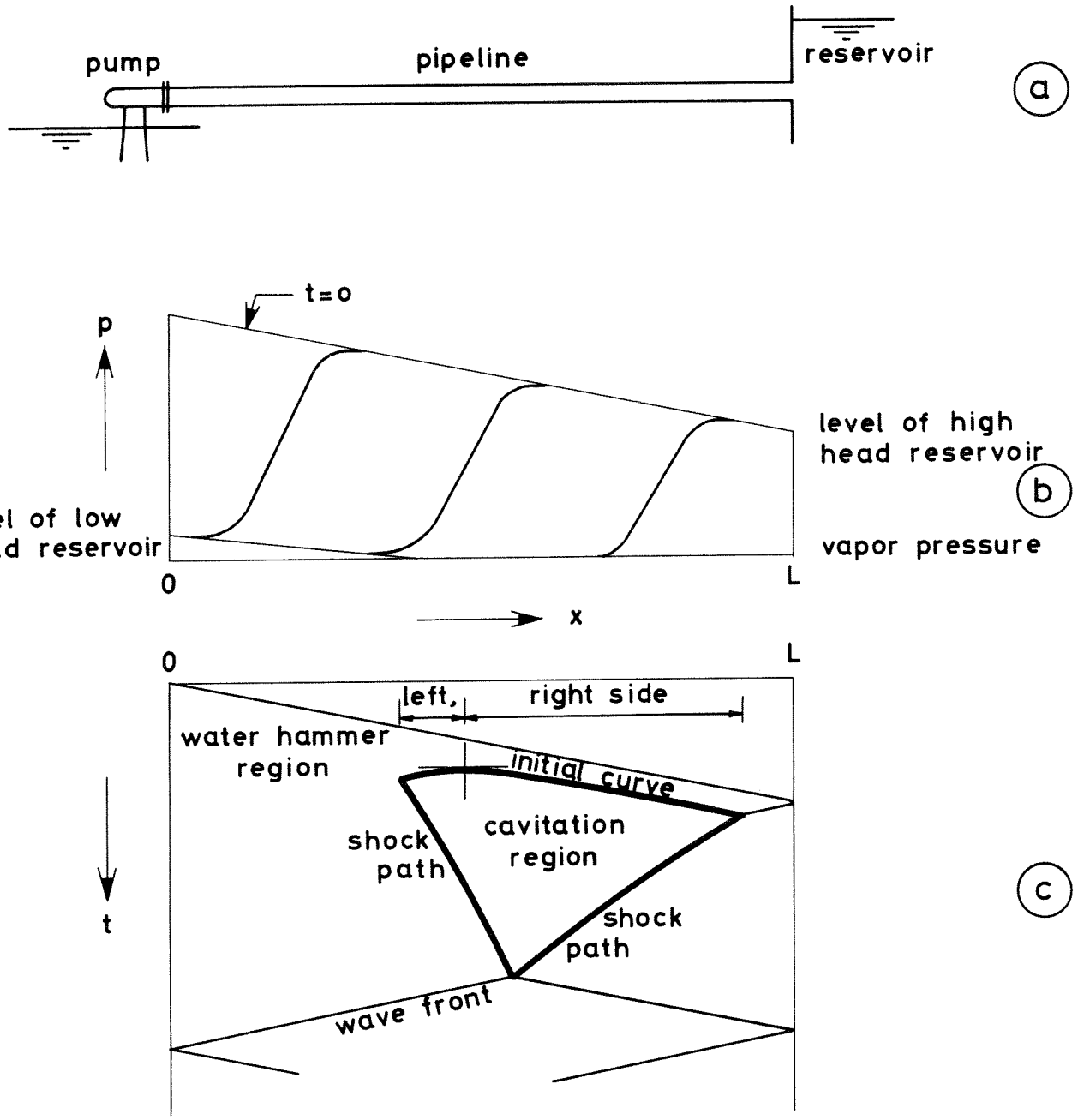

FIG. 14-PIPELINE SYSTEM WITH p,x-DIAGRAM AND x,t-DIAGRAM

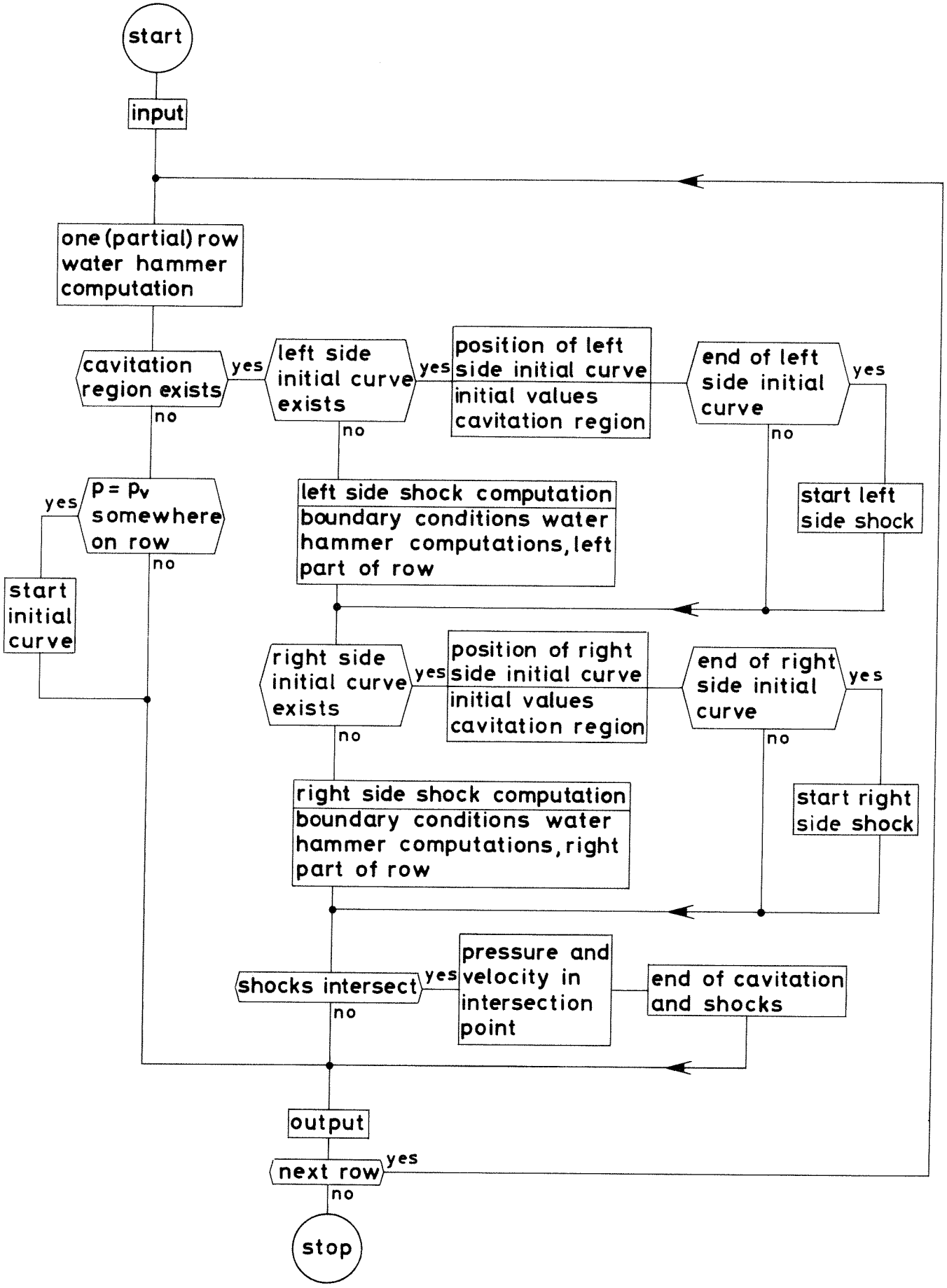

FIG.15- SIMPLIFIED FLOW CHART OF THE NUMERICAL PROGRAM

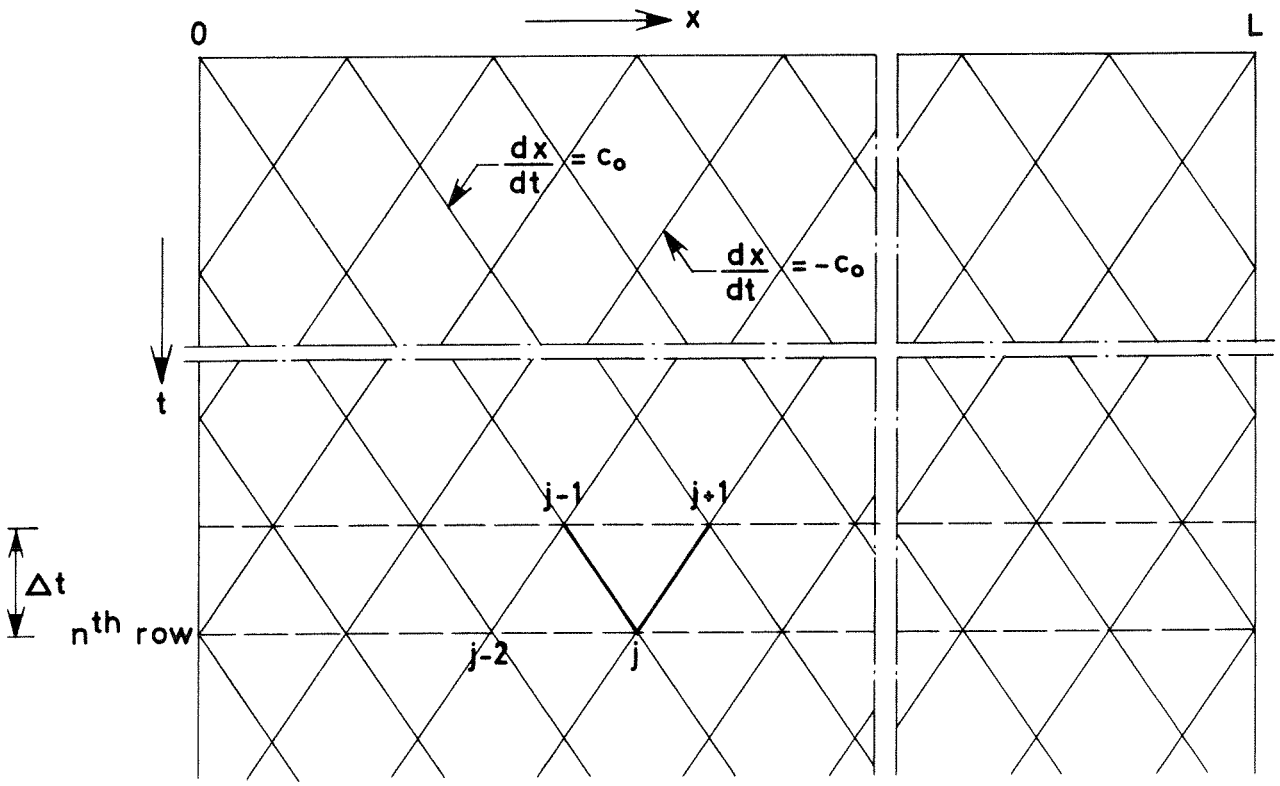

FIG. 16–LATTICE OF CHARACTERISTICS

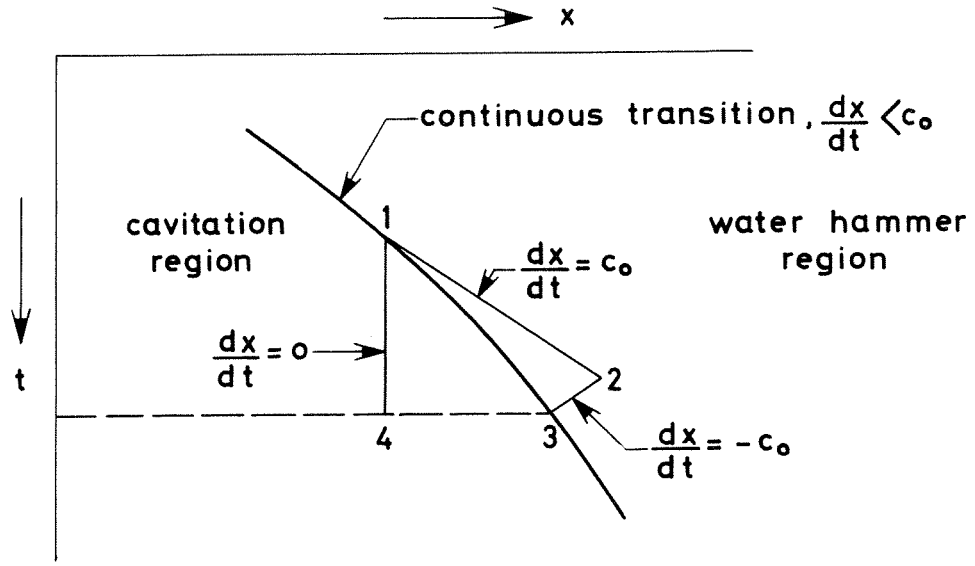

FIG. 17–EXISTENCE OF INITIAL CURVE

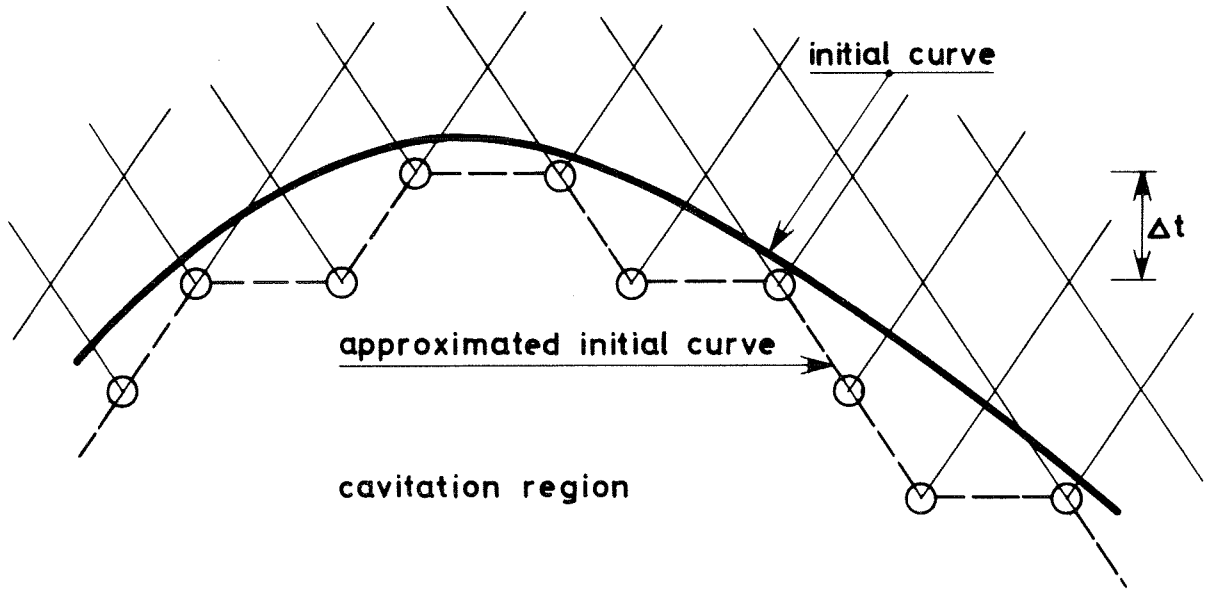

FIG. 18 – APPROXIMATION OF INITIAL CURVE

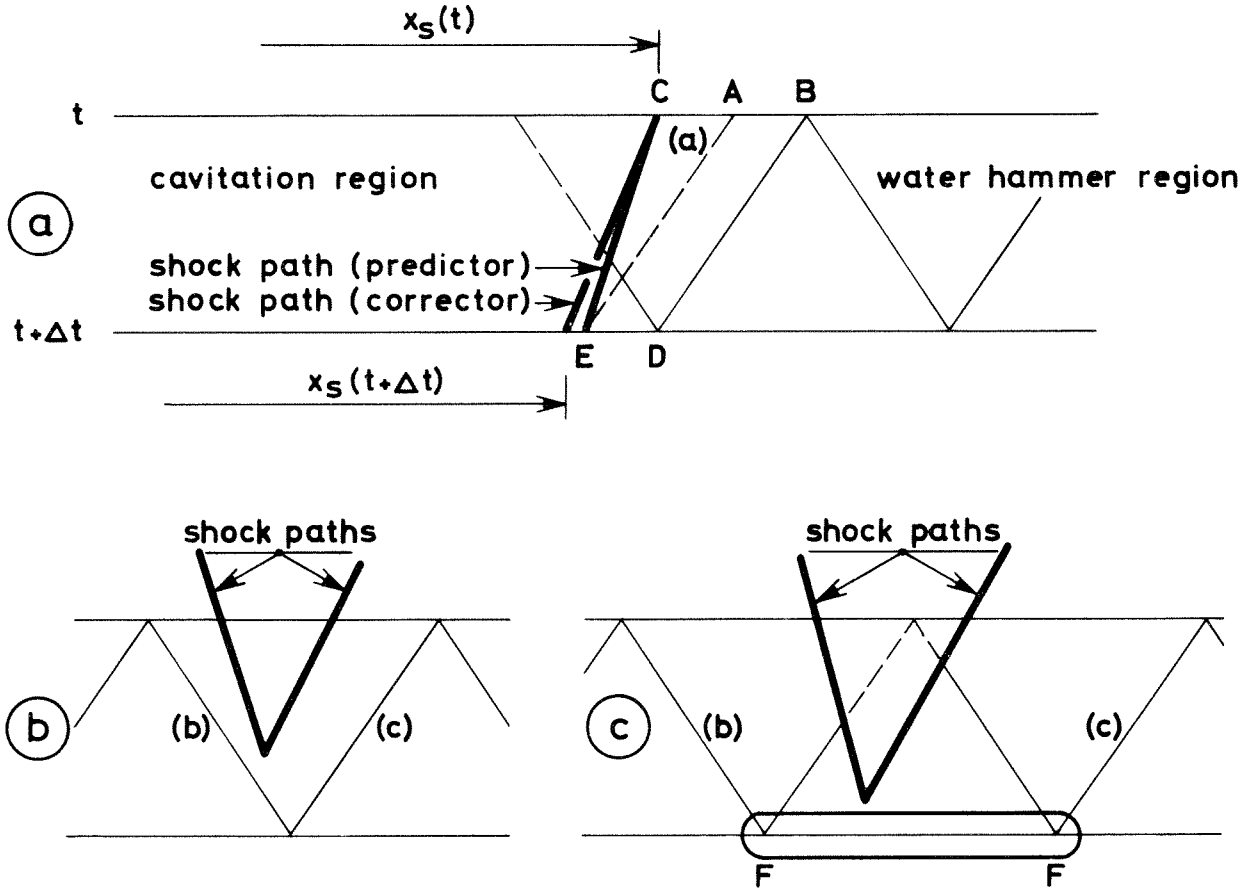

FIG. 19 – COMPUTATION OF SHOCKS

INTERNATIONAL CONFERENCE ON
PRESSURE SURGES
6th - 8th September 1972

THE EFFECT OF FREE GAS ON CAVITATION IN PIPELINES INDUCED BY WATER HAMMER

C. Kranenburg

Laboratory of Fluid Mechanics, Department of Civil Engineering.

Delft University of Technology, The Netherlands.

Summary.

A mathematical model concerning water hammer in long pipelines is presented in the case where the pressure reaches the vapour pressure of the liquid transported. Attention is principally paid to the appearance of cavitation in extensive parts of horizontal or inclined pipelines, but also column separation is dealt with. The model, which is an extension of a version published previously by J. P. Th. Kalkwijk and the author, is based on the bubble flow regime, and takes into account the influence of the release of dissolved gas. Results of numerical computations show good agreement with experimental results. The rapid attenuation of pressure surges after the occurrence of cavitation is explained.

Held at the University of Kent, Canterbury, England.
Sponsored and organised by BHRA Fluid Engineering, Cranfield, Bedford, England in conjunction with The City University, London.

NOMENCLATURE

A area of cross section
a wave celerity
c dissolved-gas concentration
D pipe diameter
E modulus of elasticity of pipe-wall material
g acceleration due to gravity
K modulus of compressibility of liquid
k universal gas constant (= 8.3J/mole/^{o}K)
L characteristic length of gas-liquid interface
ℓ length of pipeline
N number of moles of gas
n number of bubbles in a pipeline section of unit length
Pe Péclet number
p absolute pressure
R bubble radius
S surface
T absolute temperature
t time coordinate
U characteristic velocity of liquid with respect to gas-liquid interface
u liquid velocity
w pipe-wall thickness
x coordinate along axis of pipeline
α local void fraction
$\bar{\alpha}$ cross-section averaged void fraction
β diffusion coefficient
γ constant in Henry's law (= 7.0×10^{-6}moles/J for air-water at 20^{o}C)
Δ increase of a variable across a shock wave
λ wall-friction coefficient
ρ density
σ surface tension
φ angle of inclination of pipeline

Subscripts

b bubble
c cavitation
g gas
ℓ liquid
s shock wave
t top of cross-section of pipeline
v vapour
o initial condition

1. INTRODUCTION

In a pipeline transporting a liquid, a negative pressure wave may reduce the pressure to the vapour pressure of the liquid, resulting in cavitation in some part of the pipeline. If cavitation occurs in a high point for instance, then a big cavity may develop in that point, leading to column separation (Ref.1). However, cavitation may also take place in extensive horizontal or inclined parts of the pipeline, due to a gradually decreasing steady-state pressure ahead of the negative wave. In this case neither the assumption of column separation is justified, nor the exact position of cavitation occurrence is known in advance. During the appearance of sufficiently low pressures small bubbles are formed from cavitation nuclei being present in natural liquids (Ref. 2). As soon as the pressure falls below the saturation pressure of the liquid, these bubbles are going to grow due to the diffusion of dissolved gas towards the bubbles. The effect of released gas may be of importance in the case of long discharge lines, in which cavitation of the type mentioned may last many seconds.
In general, the pressures at one end or both ends of the pipeline are above vapour pressure, which in course of time results in positive pressure waves entering the region with cavitation. These waves diminish the length of this region, and eventually close it. In many cases the closure of a region with cavitation results in a sudden pressure rise which exceeds the local steady-state pressure (Ref. 3).
A summary of existent literature on this subject can be found in Ref. 4, while additional information is given in Refs. 1, 3 and 5. In the present paper a mathematical model describing the aforementioned type of cavitation, is presented. The model, which is an extension of a version published previously by Kalkwijk and Kranenburg (Refs. 4 and 6), is based on the bubble flow regime. The dependence of the wave celerity on pressure and the effect of gas diffusion towards individual bubbles are taken into account. Results of numerical computations are compared with those of an experiment in a horizontal pipeline, also described in Refs. 4 and 6. Attention is paid to the rapid attenuation of pressure surges after the occurrence of cavitation or low pressures.

2. MATHEMATICAL MODEL

2.1. Formulation

The mathematical model is based on a one-dimensional approach to the three-phase gas-vapour-liquid flow. The gravity term due to the density gradient of the mixture along the pipeline is neglected. This means that internal gravity waves do not appear in the model. This schematization is permitted, as the celerity of these waves is substantially less than the celerity of water-hammer waves.
Cavitation nuclei, which are assumed to be present in the liquid, produce gas bubbles when the pressure lowers. Below the saturation pressure of the liquid these bubbles grow due to gas diffusion and rise to the top of the pipe cross-section. As in natural liquids a large number of nuclei is present (Ref. 2), many bubbles are generated, which leads to coalescence of bubbles in the top of the cross-section. At column separations this process results in a completely separated (free surface) flow. However, as in long discharge lines the length of column separations proves to be negligibly small compared to the total length of the pipeline (Ref. 1), a column separation has little influence on the total amount of gas released from the liquid. In the remaining part of the pipeline the bubble flow regime prevails (Ref. 7) owing to the small void-fraction (Refs. 1, 4, 8 and 9), while at high pressures the voids may be present in the form of cavitation nuclei. Therefore, the prediction of gas release from the liquid will be based on the bubble flow regime for the whole pipeline. The number of bubbles in a pipeline section of unit length is assumed to be constant in place and time. Further assumptions as to the bubbles are: isothermal behaviour of the gas in the bubbles (Ref. 10), constant vapour pressure, spherical shape,

dynamic equilibrium, and same size in a cross-section.
As the celerity of water-hammer waves depends on the liquid pressure due to the presence of gas bubbles, shock waves may occur. The above assumptions concerning the bubble behaviour do not hold at shock waves.

2.2. Conservation laws

Neglecting the mass of the gas and vapour phases, application of the law of conservation of mass to the fluid in a pipeline element yields

$$\frac{\partial}{\partial t}\int_A (1-\alpha)\rho_\ell \, dA + \frac{\partial}{\partial x}\int_A (1-\alpha)\rho_\ell u \, dA = 0 \tag{1}$$

With the well-known relationships for area A of the circular pipe cross-section and liquid density ρ_ℓ (Ref. 11)

$$\frac{dA}{d p_t} = \frac{A}{\frac{w}{D}E} \tag{2}$$

and

$$\frac{d\rho_\ell}{d p_t} = \frac{\rho_\ell}{K} \tag{3}$$

in which p_t is the liquid pressure in the top of the pipe cross-section, Eq. 1 transforms to the equation of continuity

$$\frac{1}{\rho_\ell a_\ell^2}\left(\frac{\partial p_t}{\partial t} + u\frac{\partial p_t}{\partial x}\right) - \frac{1}{1-\bar{\alpha}}\left(\frac{\partial \bar{\alpha}}{\partial t} + u\frac{\partial \bar{\alpha}}{\partial x}\right) + \frac{\partial u}{\partial x} = 0 \tag{4}$$

in which

$$\bar{\alpha} = \frac{1}{A}\int_A \alpha \, dA \tag{5}$$

and

$$\frac{1}{\rho_\ell a_\ell^2} = \frac{1}{K} + \frac{\frac{w}{D}}{E} \tag{6}$$

Application of the law of conservation of momentum to the same element yields, again neglecting the mass of the gas and vapour phases

$$\frac{\partial}{\partial t}\int_A (1-\alpha)\rho_\ell u \, dA + \frac{\partial}{\partial x}\int_A (1-\alpha)\rho_\ell u^2 dA + \int_A \frac{\partial p}{\partial x} dA = -\int_A (1-\alpha)\rho_\ell \frac{\lambda}{2D} u|u| \, dA - \int_A (1-\alpha)\rho_\ell g \sin\varphi \, dA \tag{7}$$

Using Eqs. 2, 3, 4, 5 and 6, Eq. 7 changes to the equation of motion

$$\frac{\partial u}{\partial t} + u\frac{\partial u}{\partial x} + \frac{1}{\rho_\ell(1-\bar{\alpha})}\frac{\partial p_t}{\partial x} = -\frac{\lambda}{2D}u|u| - g\sin\varphi \tag{8}$$

It is noted that the usual equations of continuity and motion for water hammer are obtained, if $\bar{\alpha} = 0$ is substituted into Eqs. 4 and 8. The law of conservation of energy is replaced by the assumptions of constant vapour pressure and isothermal bubble behaviour.

2.3. The bubble suspension

The treatment of the bubble suspension is based on the properties of a single bubble. The equilibrium condition for a spherical bubble reads

$$\rho_\ell = p_v + p_g - \frac{2\sigma}{R} \tag{9}$$

Surface tension plays a role when the liquid pressure is close to vapour pressure and consequently during cavitation. The gas pressure p_g is obtained from the ideal-gas law

$$p_g \, \frac{4}{3}\pi R^3 = N_b \, kT \tag{10}$$

The relationship between pressure and bubble radius following from Eqs. 9 and 10 is discussed in Refs. 2 and 4. Concerning the occurrence of cavitation one can demonstrate that the system consisting of a large number of bubbles in a liquid, is unstable in the presence of finite but small pressure fluctuations as soon as the liquid pressure falls below vapour pressure. In the present case pressure fluctuations occur due to turbulence. A stable situation in the case of pressures below vapour pressure is obtained if it is assumed that locally only one bubble grows to a big vapour bubble, while the sizes of the remaining gas bubbles varies only slightly (Ref. 6). The effect of surface tension on the vapour bubble is small owing to the small curvature of the surface, so that after decay of dynamic transients accompanying the growth of the vapour bubble, the liquid pressure tends to vapour pressure. Also the gas density in the vapour bubbles is small, and therefore the gas content of these bubbles is negligible. Further increase of the vapour volume does not change the pressure. The part of the pipeline in which these phenomena occur will be designated as cavitation region, and the remaining part as water-hammer region. The pressure in a cavitation region is equal to vapour pressure,

$$p_{tc} = p_v \tag{11}$$

In the water-hammer region only gas bubbles exist, which gives the following expression for the average void-fraction

$$\bar{\alpha}_g = \frac{4}{3}\pi \frac{n}{A} R^3 \tag{12}$$

Subscript g has been added as only gas bubbles are concerned. In the cavitation region gas and vapour bubbles occur. Therefore, in this case it is convenient to divide the total void-fraction into two parts accounting for gas bubbles and vapour voids, respectively,

$$\bar{\alpha}_c = \bar{\alpha}_g + \bar{\alpha}_v \tag{13}$$

The void fraction concerning gas bubbles ($\bar{\alpha}_g$) in Eq. 13 satisfies Eq. 12.

The diffusion of gas in a liquid is caused by a gradient of the concentration of dissolved gas. The mass flux of gas through a surface S which is connected to the liquid particles, is given by Fick's first law

$$\frac{dN}{dt} = \int_S \beta \frac{\partial c}{\partial \nu} dS \tag{14}$$

in which ν is the coordinate, normal to the surface S. The equilibrium concentration c_b on a gas-liquid interface follows from Henry's law

$$c_b = \gamma p_g \tag{15}$$

The parameter which determines the character of the diffusion process is the Péclet number

$$Pe = \frac{LU}{\beta} \tag{16}$$

The Péclet number is the equivalent for gas diffusion of the Reynolds number characterizing the diffusion of vorticity in laminar flow. Assuming

$$U \sim 0.01\text{m/s}, \quad L \sim 10^{-3}\text{m}, \quad \beta = 2\times10^{-9}\text{m}^2/\text{s} \text{ (air-water at } 20^\circ\text{C)}$$

one obtains $Pe \sim 5\times10^3$. This large value of the Péclet number indicates that gas diffusion occurs mainly in a boundary layer with thickness $\sim L/\sqrt{Pe}$ along the bubble wall, as is pointed out by Levich (Ref. 12). In this case, from Ref. 12 also an approximate solution can be obtained for a spherical bubble which moves in an inviscid liquid. The expression for the mass flux towards a bubble according to this solution, which was also obtained by Boussinesq, reads

$$\frac{dN_b}{dt} = (c_o - c_b)\sqrt{32\pi U R^3} \tag{17}$$

in which c_o is the constant gas concentration at some distance from the bubble. A differential equation for the bubble radius as a function of time can be obtained using Eqs. 10 and 9 and Henry's law, Eq. 15. In the simple case where the liquid pressure is equal to vapour pressure and the concentration on the bubble wall c_b is negligible, one obtains after integration, assuming $R(o) \approx 0$

$$R(t) = \frac{1}{2\pi} \beta U \left(\frac{3}{4} \frac{kTc_o}{\sigma} t \right)^2 \tag{18}$$

For water which is saturated at atmospheric pressure ($kTc_o = 1700 N/m^2$), surface tension $\sigma = 0.073$ N/m, and a (small) slip velocity $U = 0.01$m/s from Eq. 18 the bubble radius is found to amount to $R = 0.25 \times 10^{-3}$m after 0.5s and to $R = 10^{-3}$m after 1s. This example illustrates the fast bubble growth at vapour pressure.
The celerity of a disturbance in the water-hammer region can be obtained from the expression

$$a^2 = \frac{dp}{d\rho} \tag{19}$$

which yields in this case

$$\frac{1}{a^2} = \frac{1}{A} \frac{d}{dp_t} \left[(1 - \bar{\alpha}_g) \rho_l A \right]_{N_b = \text{constant}} \tag{20}$$

After differentiation one obtains

$$\frac{1}{a^2} = (1 - \bar{\alpha}_g) \left(\frac{1}{\rho_l} \frac{d\rho_l}{dp_t} + \frac{1}{A} \frac{dA}{dp_t} \right) - \left[\frac{d\bar{\alpha}_g}{dp_t} \right]_{N_b = \text{constant}} \tag{21}$$

Substitution of Eqs. 2 and 3, and differentiation of $\bar{\alpha}_g$ with respect to p_t, using Eqs. 9, 10 and 12, yields

$$\frac{1}{\rho_l a^2} = \frac{1 - \bar{\alpha}_g}{\rho_l a_l^2} + \frac{\bar{\alpha}_g R^3}{\frac{3}{4\pi} N_b kT - \frac{2}{3} \sigma R^2} \tag{22}$$

The values of celerity a, obtained from Eq. 22, are less than the celerity a_l in the absence of free gas. Celerity a decreases when the pressure decreases, but remains greater than zero when the pressure tends to vapour pressure.

2.4. Simplified equations of continuity and motion

As was pointed out, the void fraction in the water-hammer region is small so that in Eqs. 4 and 8 it can be neglected with respect to unity. Moreover, the convective terms can be neglected (Refs. 5 and 11). Thus for the water-hammer region the simplified equations of continuity and motion

$$\frac{1}{\rho_l a_l^2} \frac{\partial p_t}{\partial t} - \frac{\partial \bar{\alpha}_g}{\partial t} + \frac{\partial u}{\partial x} = 0 \tag{23}$$

$$\frac{\partial u}{\partial t} + \frac{1}{\rho_l} \frac{\partial p_t}{\partial x} = - \frac{\lambda}{2D} u|u| - g \sin \varphi \tag{24}$$

are obtained. In the cavitation region Eqs. 4 and 8 simplify due to the constant-pressure condition (Eq. 11), while the convective terms are negligible again. The total void-fraction, however, may reach values which have the order of magnitude of unity at column separations. These considerations lead to the simplified equations of continuity and motion for the cavitation region

$$\frac{1}{1 - \bar{\alpha}_c} \frac{\partial \bar{\alpha}_c}{\partial t} - \frac{\partial u}{\partial x} = 0 \tag{25}$$

$$\frac{\partial u}{\partial t} = - \frac{\lambda}{2D} u|u| - g \sin \varphi \tag{26}$$

The influence of a large void-fraction on wall friction has been neglected. The total void-fraction in the cavitation region is determined by Eqs. 25 and 26,

while the gas fraction follows from Eqs. 9, 10, 12 and 17 for the gas-bubble suspension.

2.5. Shock waves, Transition from water-hammer to cavitation region

The celerity in the water-hammer region depends on the pressure. Consequently, during the propagation of a positive pressure wave the wave front steepens, eventually resulting in the development of a shock wave. The thickness of this shock wave is determined by dynamic and thermodynamic bubble effects. Neglect of these effects leads to a discontinuous wave, but nevertheless the overall shock behaviour is described well (Ref. 13). The derivation of the shock relations, which is based on the application of the laws of conservation of mass and momentum across the shock, is completely analogous to that given in Ref. 4. Therefore, only the results are given herein:

$$\Delta p_t = \rho_\ell \, a_s \, \Delta u \tag{27}$$

$$\frac{1}{\rho_\ell a_s^2} = \frac{1}{\rho_\ell a_\ell^2} - \frac{\Delta \bar{\alpha}}{\Delta p_t} \tag{28}$$

in which a_s is the shock-wave celerity, Δp_t is the increase of pressure across the shock ($\Delta p_t > 0$ by definition), $\Delta \bar{\alpha}$ is the increase of total void-fraction across the shock ($\Delta \bar{\alpha} < 0$), and Δu is the increase of velocity across the shock. The condition that the internal energy of the fluid cannot decrease during passage of a shock (Ref. 13) yields $a_s > 0$ and $\Delta u > 0$ (the liquid velocity is chosen positive in the direction of shock propagation) so that only compression shocks are possible. If the shock strength Δp_t reduces to zero, then Eq. 28 changes to Eq. 22, neglecting $\bar{\alpha}_g$ with respect to unity, for the celerity of a small disturbance.
During the genesis of a cavitation region, celerity a_c of the transition from water-hammer to cavitation region appears to be greater than the local celerity at vapour pressure in the water-hammer region. It can be shown that a shock wave starts to build up on the transition, when celerity a_c decreases to the celerity at vapour pressure. As soon as this occurs, the direction of propagation of the transition is reversed, the shock penetrates into the cavitation region, thus closing it (Ref. 6). The shock relations, Eqs. 27 and 28, also apply to this case. Another possibility as to the termination of cavitation is the growth of gas bubbles due to the release of dissolved gas. The growth rate of the gas bubbles increases during cavitation owing to increase of the sizes of the bubbles, while the growth rate of the total void-fraction decreases due to wall friction. Cavitation terminates as soon as $\bar{\alpha}_g = \bar{\alpha}_c$. Hereafter, gas diffusion continues and, if no other influences are present, the liquid pressure begins to rise above vapour pressure. However, this situation is not always reached owing to the aforementioned propagation of shock waves on the boundaries of the cavitation region.
As an example of the behaviour of the transition, in Fig. 1 the appearance of a cavitation region after pump failure which induces a negative pressure wave in the horizontal pipeline, is shown. During the genesis of this region the transition is continuous. Next, shock waves are formed which start to close the cavitation region.

2.6. Numerical computations

The equations of continuity and motion for the water-hammer region, Eqs. 23 and 24, are integrated numerically, using the Lax-Wendroff two-step scheme (Ref. 14), which permits the occurrence of shock waves. The numerical smoothing of these shock waves is accompanied by oscillations, which are undesirable in the present case as vapour pressure might be reached erroneously. The oscillations could be suppressed using an additional filtering operator (Ref. 15). Eqs. 23 and 24 can be written as conservation laws, which is a requirement using the

scheme mentioned. Strictly speaking, the momentum equation should be used instead of the equation of motion in view of the occurrence of shocks. The differences are small, however, as the liquid velocity is substantially less than the shock celerity.
A special shock type occurs on the boundaries of a cavitation region. In this case different systems of equations hold on both sides of the shock wave. As moreover the description of the development and closure of the cavitation region is a main topic of the present investigation, this shock type is calculated using a shock-fitting procedure (Eqs. 27 and 28), which is more accurate.
As soon as during the computation the pressure reaches vapour pressure somewhere in the pipeline, the development of a cavitation region is started in the numerical programme. During genesis of cavitation, initial conditions are computed which are needed in the analytical solution of the equations for the cavitation region, Eqs. 25 and 26 (Ref. 4). In a later phase of the computation, when a shock has built up on a boundary of the cavitation region, this solution is used in the shock-fitting procedure (Ref. 6).

3. COMPARISON OF COMPUTATIONS WITH EXPERIMENT

3.1. Description of model pipeline

The model pipeline for which computations have been made, is described elsewhere (Ref. 4). Therefore, only some important features will be mentioned herein. The model is depicted schematically in Fig. 2. The horizontal pipeline, transporting tap water, consists of polyvinyl chloride. In the steady-state situation the water flows from a high-head to a low-head reservoir. The levels in the reservoirs are constant during an experiment. Cavitation is induced in the pipeline by the momentaneous closure of a piston valve at the upstream end of the pipeline. The steady-state discharge and the transient pressures at some points of the pipeline could be measured.

3.2. Experiment

The closure of the piston valve causes column separation behind the valve, and a negative pressure wave starts to propagate in the downstream direction. Due to the steady-state friction gradient a cavitation region is generated at the rear of this wave. The steepness of the wave decreases during propagation. Reflection of the negative wave at the low-head reservoir results in a positive pressure wave propagating in upstream direction. This wave, in which a very steep part or shock develops, removes the cavitation region. After passage of the wave, small gas bubbles remain behind, demonstrating the effect of gas release from the liquid. When the positive wave reaches the column separation behind the valve, it is reflected again, but a cavitation region is not generated anymore. The waves damp fast so that after some reflections the water in the pipeline behaves as a rigid column. During this process the velocity changes its direction, finally resulting in collapse of the column-separation cavity. At this moment the experiment was ended.

3.3. Computation

The numerical values of the relevant quantities were adopted from the model, such as celerity a_f = 430m/s, friction coefficient λ = 0.0194, steady-state velocity u_o = 0.97m/s, length ℓ = 200m, diameter D = 0.0814m, and downstream pressure p_t = 82kN/m^2. The water is assumed to be saturated at atmospheric pressure, which gives c_o = 0.70moles/m^3. The estimation of number of bubbles n and slip velocity U was based on the observation of bubbles through transparant parts fitted in the pipeline, and was rather arbitrary. However, the influence of dissolved-gas release can be seen as a second order effect so that accurate determination of n and U is not of great importance. In the computations n = 500m^{-1} and U = 0.01m/s were assumed. The initial radius of the bubbles at atmospheric pressure was assumed to amount to R_o = 3.2×10^{-5}m.

4. RESULTS AND CONCLUSIONS

In Figs. 3, 4, and 5 the experimental and computed pressure histories at some cross-sections are shown. Regarding the experimental curves it can be noted that a strong dispersion (deformation) and attenuation of the pressure waves occur, which is a well-known result (Ref. 5). Although the front of the pressure wave removing the cavitation region is steep, the gradual development of a shock wave is not clearly observed. However, at $X = 34m$ the front of the wave is almost vertical, which indicates that at this place a shock has built up. The three sets of computed curves concern a computation without the presence of free gas, a computation with bubbles containing a constant quantity of gas (no gas diffusion), and a computation in which gas diffusion was taken into account in the way pointed out in the preceding pages. In the computation mentioned first the method of characteristics was used in the water-hammer region, whereas in the second and third computation the aforementioned finite--difference method was applied. The computation without free gas does not show significant dispersion or attenuation of the pressure waves (Fig. 3). The computation with free gas but without gas diffusion does show dispersion of the waves but the strong wave attenuation is not found (Fig. 4). The little change in the steepness of the first negative pressure wave proves that the more rounded shape of the waves occurring later on is not caused by numerical smoothing, but is part of the mathematical model.
Wave attenuation is found if gas diffusion is introduced in the mathematical model (Fig. 5). The damping is considerable, in spite of the fact that a relatively small slip velocity and a reasonable number of bubbles were assumed. The attenuation is caused by the decrease of the celerity while time elapses, and by the increase of the free-gas content. This can be shown by eliminating void fraction α_g and the derivatives of the velocity u from the equations of continuity and motion, Eqs. 23 and 24. Then a non-linear telegraph equation results, the dissipation term of which contains the derivative of the celerity with respect to time and a factor related to the free-gas generation rate.
The conclusions are that free gas causes wave dispersion, and that the strong wave attenuation observed after cavitation and the occurrence of low pressures, can be explained by the effects of gas diffusion.

REFERENCES

1. Tanahashi, T. and Kasahara, E.:"Comparisons between experimental and theoretical results of the waterhammer with water column separation ".Bull. Jap. Soc. Mech. Engrs.,13,61,pp.914-925.(1970).
2. Knapp, R.T., Daily, J.W. and Hammitt, F.G.:"Cavitation". McGraw-Hill.(1970).
3. Vreugdenhil, C.B., de Vries, A.H., Kalkwijk, J.P.Th., and Kranenburg, C.: "Investigation into cavitation in long horizontal pipelines caused by water-hammer". Proc. 6th Symposium of the IAHR. Organized by the Section for hydraulic machinery, equipment and cavitation of the Int. Ass. of Hydr. Res.. Rome, Italy.(1972).
4. Kalkwijk, J.P.Th. and Kranenburg, C.:"Cavitation in horizontal pipelines due to water hammer". J. Hydr. Div., ASCE, 97,HY10,pp.1585-1605.(1971).
5. Weyler, M.E., Streeter, V.L. and Larsen, P.S.:"An investigation of the effect of cavitation bubbles on the momentum loss in transient pipe flow". J. Basic Engng., ASME, 93,1,pp.1-10.(1971).
6. Kalkwijk, J.P.Th. and Kranenburg, C.:"Cavitation in horizontal pipelines due to water hammer". Report No. B/71/3, Delft University of Technology, Dept. of Civ. Engng., Lab. of Fluid Mech..(1971).
7. Wallis, G.B.:"One-dimensional two-phase flow". McGraw-Hill.(1969).
8. Dijkman, H.K.M. and Vreugdenhil, C.B.:"The effect of dissolved gas on cavitation in horizontal pipe-lines". J. Hydr. Res.,7,3,pp.301-314.(1969).
9. de Haller, P. and Bédué, A.:"The break-away of water columns as a result of negative pressure shocks". Sulzer Techn. Rev.,4,pp.18-25.(1951).
10. Hsieh, D.Y. and Plesset, M.S.:"On the propagation of sound in a liquid containing gas bubbles". Physics of Fluids,4,8,pp.970-975.(1961).

11. Parmakian, J.:"Waterhammer analysis". Dover.(1963).
12. Levich, V.G.:"Physicochemical hydrodynamics". Prentice-Hall.(1962).
13. Campbell, I.J. and Pitcher, A.S.:"Shock waves in a liquid containing gas bubbles". Proc. Roy. Soc.,A243,pp.534-545.(1958).
14. Richtmeyer, R.D. and Morton, K.W.:"Difference methods for initial-value problems". Interscience.(1967).
15. Vliegenthart, A.C.:"The Shumann filtering operator and the numerical computation of shock waves". J. Engng. Math.,4,4,pp.341-348.(1970).

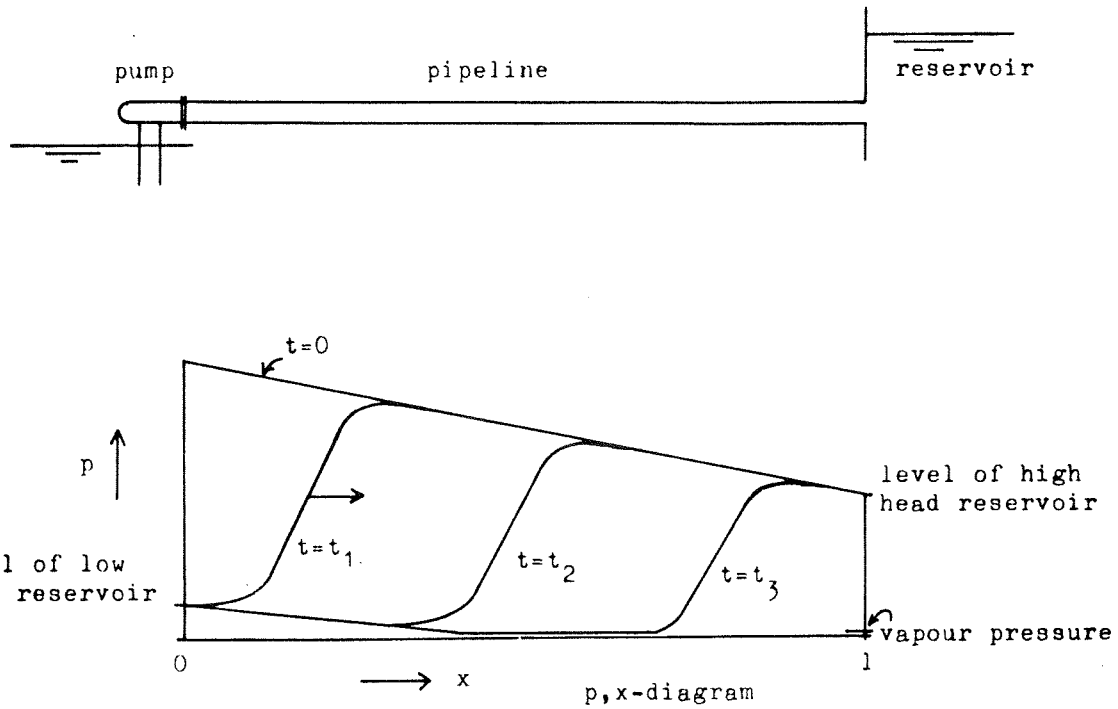

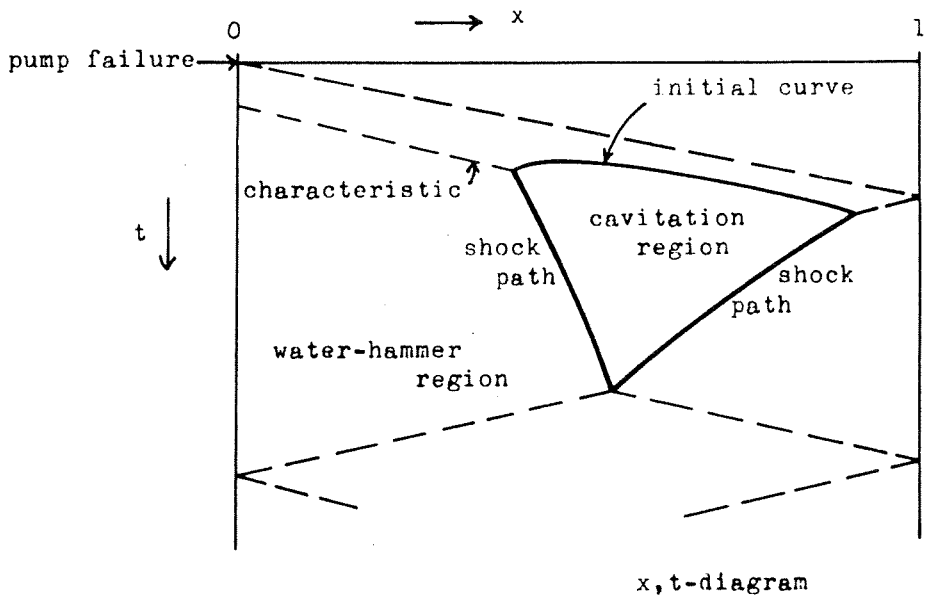

Fig. 1 Example of cavitation occurrence after pump failure.

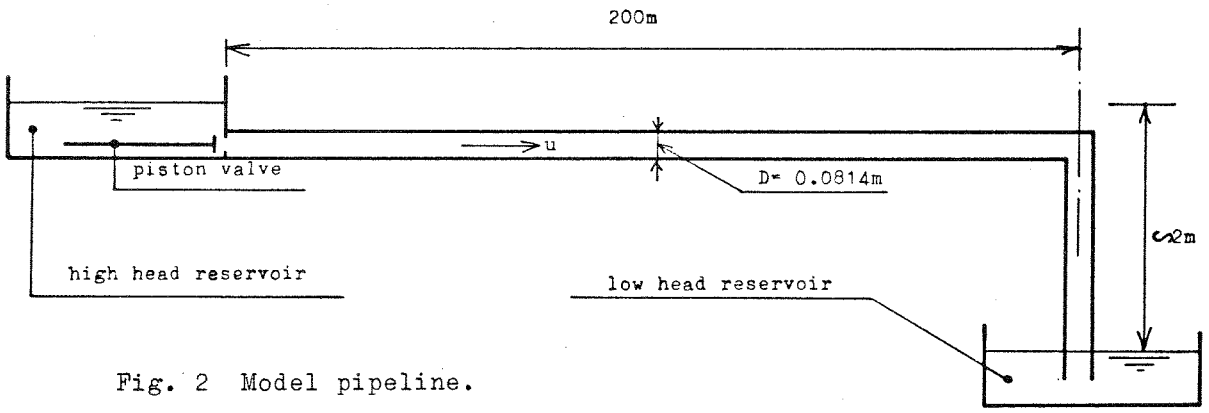

Fig. 2 Model pipeline.

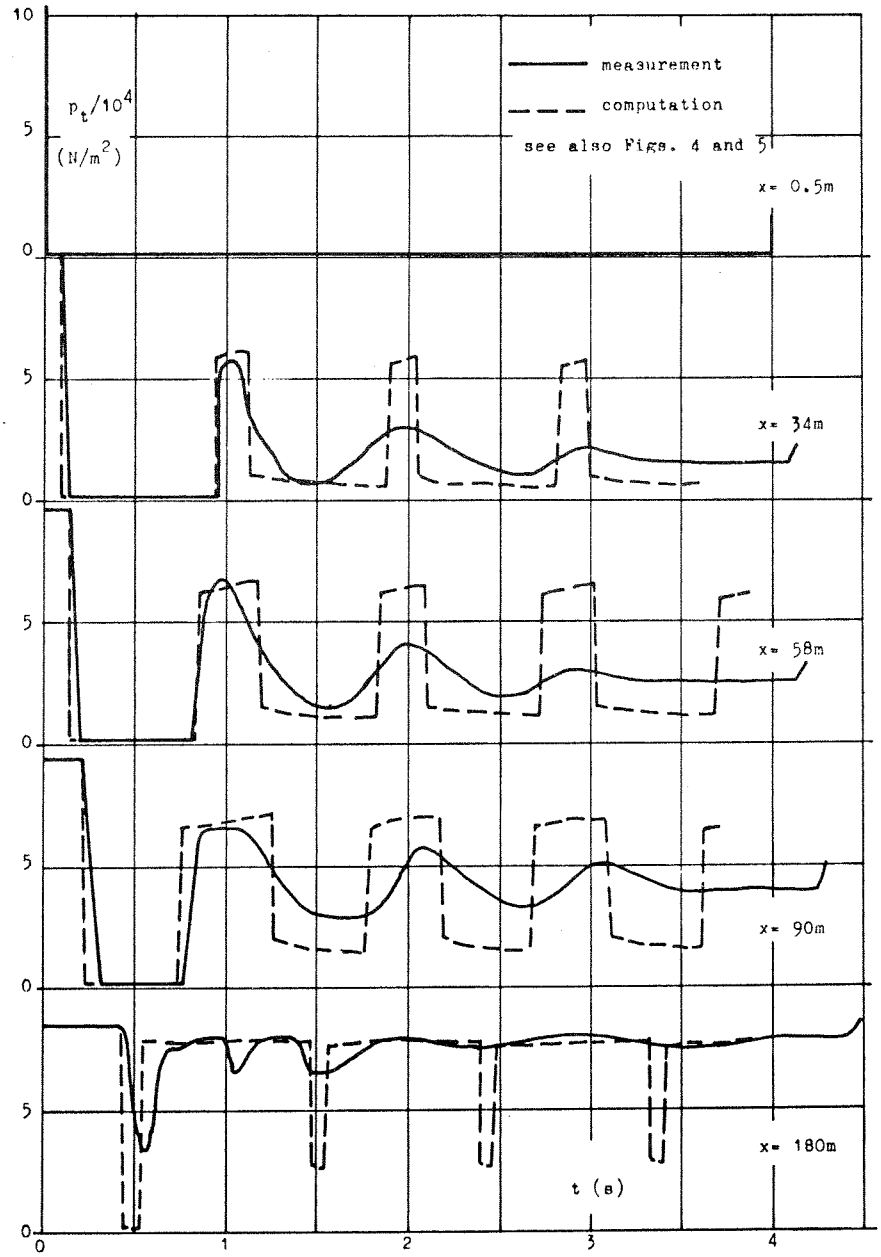

Fig. 3 Pressure histories at 0.5, 34, 58, 90 and 180m from the upstream end of the pipeline. Computation without free gas.

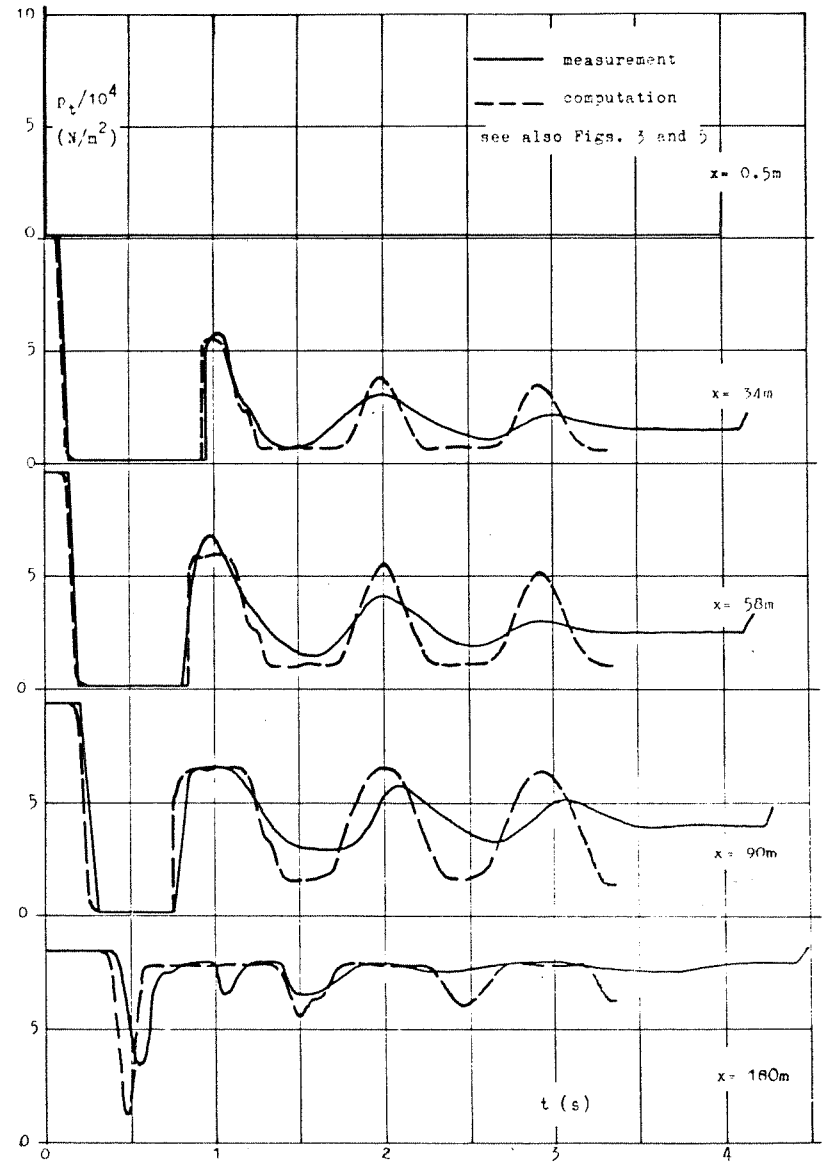

Fig. 4 Pressure histories at 0.5, 34, 58, 90 and 180m from the upstream end of the pipeline. Computation with bubbles containing a constant quantity of free gas.

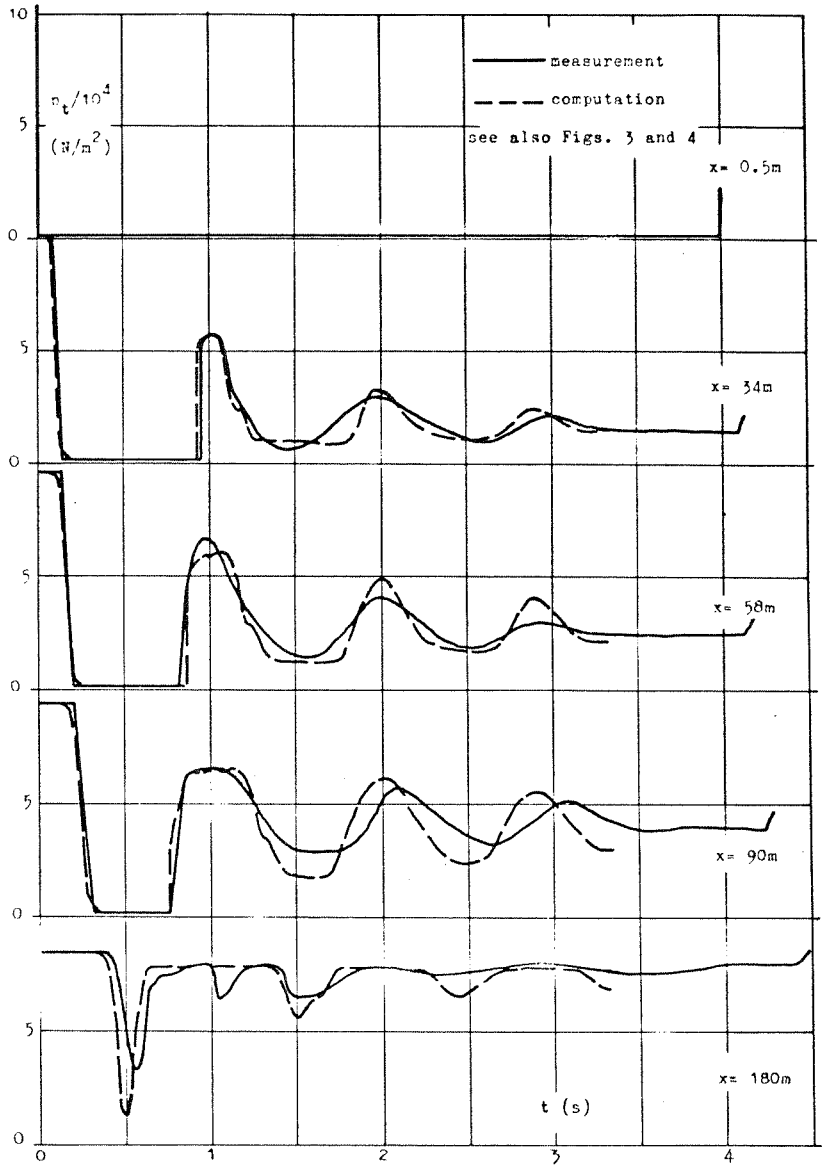

Fig. 5 Pressure histories at 0.5, 34, 58, 90 and 180m from the upstream end of the pipeline. Computation with gas diffusion.